Lawrence Berkeley National Laboratory
Applied Math & Comp Sci

Title
"Dense diffusion" in colloidal glasses: short-ranged long-time self-diffusion as a mechanistic model for relaxation dynamics

Authors
Wang, J Galen
Li, Qi
Peng, Xiaoguang
et al.

Soft Matter

Accepted Manuscript

Volume 13
Number 45
7 December 2017
Pages 8341-8662

Soft Matter

rsc.li/soft-matter-journal

ISSN 1744-6848

ROYAL SOCIETY
OF CHEMISTRY

PAPER
Kerstin Baumgarten and Brian P. Tighe
Viscous forces and bulk viscoelasticity near jamming

ROYAL SOCIETY
OF CHEMISTRY

rsc.li/soft-matter-journal

Soft Matter

ARTICLE TYPE

"Dense diffusion" in colloidal glasses: short-ranged long-time self-diffusion as a mechanistic model for relaxation dynamics

J. Galen Wang,[a] Qi Li,[b] Xiaoguang Peng,[c] Gregory B. McKenna,[b] and Roseanna N. Zia[*a]

Despite decades of exploration of the colloidal glass transition, mechanistic explanation of glassy relaxation processes has remained murky. State-of-the-art theoretical models of the colloidal glass transition such as Random First Order Transition theory, Active Barrier Hopping theory, and Non-equilibrium Self-consistent Generalized Langevin theory assert that relaxation reported at volume fractions above the ideal Mode Coupling Theory prediction $\phi_{g,MCT}$ requires some sort of activated process, and that cooperative motion plays a central role. However, discrepancies between predicted and measured values of ϕ_g and ambiguity in the role of cooperative dynamics persist. Underlying both issues is the challenge of conducting deep concentration quenches without flow and the difficulty in accessing particle-scale dynamics. These two challenges have led to widespread use of fitting methods to identify divergence, but most *a priori* assume divergent behavior; and without access to detailed particle dynamics, it is challenging to produce evidence of collective dynamics. We address these limitations by conducting dynamic simulations accompanied by experiments to quench a colloidal liquid into the putative glass by triggering an increase in particle size, and thus volume fraction, at constant particle number density. Quenches are performed from the liquid to final volume fractions $0.56 \leq \phi \leq 0.63$. The glass is allowed to age for long times, and relaxation dynamics are monitored throughout the simulation. Overall, correlated motion acts to release dynamics from the glassy plateau — but only over length scales much smaller than a particle size — allowing self-diffusion to re-emerge; self-diffusion then relaxes the glass into an intransient diffusive state, which persists for $\phi < 0.60$. We observe similar relaxation dynamics up to $\phi = 0.63$ before achieving the intransient state. We find that this long-time self-diffusion is short-ranged: analysis of mean-square displacement reveals a glassy cage size a fraction of a particle size that shrinks with quench depth, i.e increasing volume fraction. Thus the equivalence between cage size and particle size found in the liquid breaks down in the glass, which we confirm by examining the self-intermediate scattering function over a range of wave numbers. The colloidal glass transition can hence be viewed mechanistically as a shift in the long-time self-diffusion from long-ranged to short-ranged exploration of configurations. This shift takes place without diverging dynamics: there is a smooth transition as particle mobility decreases dramatically with concomitant emergence of a dense local configuration space that permits sampling of many configurations via local particle motion.

1 Introduction

Colloidal glasses are densely packed particulate suspensions that provide unique mechanical and optical functions in natural and engineered materials. Vitrified colloidal states are observed in paints and coatings as they cure[1–3], in the bacterial cytoplasm as a survival strategy[4] and in food stuffs[5,6], to name just a few. Like colloidal gels, glasses result when a thermodynamic phase transition fails[2]. That is, although colloidal suspensions display equilibrium phase transitions quite similar to those in molecular materials, they also display similar non-equilibrium transitions, namely gelation, a process by which liquid-gas phase separation fails[7], and vitrification, a solidification process during which crystallization fails[2]. Kinetics and aging are key to both processes; it

a Department of Chemical Engineering, Stanford University, Stanford, CA 94305, U.S.A. Email: rzia@stanford.edu

b Department of Chemical Engineering, Texas Tech University, Lubbock, TX 79409, U.S.A.

has been shown that crystallization can sometimes emerge long after vitrification[8] as can phase separation after gelation[9–11]. The failure of classical thermodynamics along the vitrification path has led to a rich literature over the last 150 years[12–40]. The aim of such work is twofold: to predict the conditions under which vitrification occurs, and to explain the same mechanistically via predictive theory.

There are many fine reviews of the colloidal glass transition literature that together detail advancement toward consensus as well as persistent open questions[2,3,41–50]. There is broad consensus that hallmarks of vitrification include dramatic slowing of relaxation timescales (whether measured directly via dynamic light scattering[30,51–53] or indirectly via rheometry[54–62]); frozen-in liquid-like structure; and that polydispersity[63–68] and interparticle potential[51,69,70] change the volume fraction at which the hallmark behaviors emerge. However, the continuous temporal evolution of transport coefficients and thermodynamic variables — e.g. in colloids, the viscosity, diffusivity, and moduli — after the quench that exemplifies vitrification underlies the most difficult open questions that remain. Among these are the questions of whether cooperative motion drives glassy relaxation[23,24,38,71–74]; whether relaxation time formally diverges and, if so, at what volume fraction[2,36,48,68,75–78]; what dynamical process enables decorrelated dynamics to continue at high volume fraction[23,25,28,35,38,78,79]; and what is the driving force for such dynamical processes[25,38,71,80]. Although there has been much effort devoted to developing a thermodynamic view of the glass transition in the region where activation is dominant, and to describing vitrification in terms of its onset and its long-time "metastable" characteristics, no theory provides a problem-free mechanistic explanation.

Putative divergent growth of relaxation time τ_{rel} or viscosity η with increasing volume fraction ϕ is often the result of a data-fitting procedure, where experimental data are fit to phenomenological models (such as the Vogel-Fulcher-Tammann (VFT) model[15–17] and the Krieger-Dougherty model[21]), in order to extrapolate to volume fractions that are inaccessible in experiments[2]. The VFT fit typically extrapolates to divergence[54,59–62] between $\phi = 0.56$ and $\phi = 0.60$, depending on polydispersity[67,68]. The shortcoming of this approach is that the model *a priori* assumes that divergent behavior exists, and then simply locates it at a specific volume fraction ϕ_{VFT}. Further, the fit is agnostic to many rate processes — it is an empirical fit to data — and mechanistic theories are needed to interpret the observed and extrapolated behaviors to give mechanistic insight into relaxation dynamics.

Formal prediction of a strict divergence of relaxation time with increasing volume fraction is obtained by the Mode-Coupling Theory (MCT), a hard-sphere model derived from conservation laws[28]. The so-called idealized MCT predicts divergence to occur at $\phi_{g,MCT} = 0.525$. While this landmark work successfully recovered the dramatic slowing of the α relaxation time (long-time self-diffusion), as well as a more and more pronounced β relaxation (corresponding to in-cage diffusion in colloids) observed in experiments of colloidal systems, it markedly under-predicts the divergence point observed in experiments, which some claim arises from MCT's neglect of thermally activated processes[48,80].

MCT thus keeps the door open to the possibility that no divergence exists prior to random close packing (RCP). *Ad hoc* modifications to MCT[75] manage to align its prediction of divergence with that inferred via fitting in experiments (e.g. van Megen and Underwood[51] find $\phi_g = 0.581$). The *ad hoc* adaptations of MCT are dissatisfying because firstly, there are any number of other equally satisfying *ad hoc* adjustments to $\phi_{g,MCT}$ that could obtain (or invalidate) the revised value, muddying the waters for mechanistic understanding. Secondly, later work by van Megen and Williams[67] showed that aging of the sample could move the divergence point, widening disagreement between MCT and experiments.

Contemporaneous development of the Random First Order Transition theory (RFOT)[35,71,76] made some headway with the under-prediction of $\phi_{g,MCT}$. RFOT was originally a spin-glass model[31–34] developed for molecular systems but has been increasingly applied to colloidal systems. RFOT encountered the same under-prediction as idealized MCT, and addressed it by connecting with a growing consensus in the literature that an activated process must exist to overcome some sort of energy barrier, as originally proposed by Goldstein[25]. This idea in itself simultaneously connected to the question of an underlying thermodynamic transition, as well as the still-open question of what mechanism enables glassy relaxation. The failure of spin-glass RFOT was hypothesized to arise from the mean-field nature of that infinite-range model, which required correlations over infinite distances that in turn presented an infinitely large barrier to activated rearrangements. The idea that real glasses are finite in extent led to a search for finite length scales over which thermally activated processes can drive structural relaxation, decorrelation, and finite relaxation time. To do so, RFOT patches together several theoretical ideas[48], borrowing the energy landscape idea from Goldstein[25], where a cooling molecular liquid explores an energy landscape as its constituent elements rearrange. RFOT envisioned a landscape with finite barriers set by finite length scales over which particle relaxation must occur; with higher volume fraction, the barriers grow, the length scales diverge, and thus a second-order *thermodynamic* glass transition is hypothesized to occur, where a discontinuity in the Edwards-Anderson order parameter also occurs (this discontinuity underlies the "first order" nature of RFOT). Relaxation is envisioned to require *cooperative* motion over these defined length scales in order for decorrelation to occur[23], which has been appealing to an informal consensus in the colloidal literature that cooperative motion drives glassy relaxation. The hypothesized activated process responsible for relaxation at $\phi > \phi_{g,MCT}$ should ostensibly reveal the sought-after mechanistic explanation of vitrification. However, the entropic driving force so proposed by the authors has been questioned[80], and alternative explanations involving surface tension of the cooperative rearranging regions[80] are equally unsatisfying. Nonetheless, the model ultimately proposes a diverging relaxation timescale, but again only by pre-supposing vanishing configurational entropy to occur at ϕ_{RCP} by enforcing the VFT model: $\tau_{rel} \sim \exp(\nu/(\phi_{RCP}/\phi - 1))$, where ϕ_{RCP} is the volume fraction at random close packing (RCP) and ν is a fitting parameter. At the very least the reliance of RFOT on an (extrapolated) ideal

glass transition that assumes divergent behavior gives a simple mandate to explore the validity of the assertion that colloidal dynamics slow divergently anywhere. If this test fails, then the flaw in applying the equilibrium theory may be unfixable, and a new approach required.

More recent attempts to frame the colloidal glass transition within an energy landscape have focused on explicitly representing particle-scale dynamics in overcoming energy barriers, and these provide more convincing estimates of relaxation dynamics. To wit, Activated Barrier Hopping Theory (ABHT)[36,37] utilizes the Langevin equation to obtain particle positions and then transforms them to a density operator. Density functional theory is used to solve the resulting conservation equation, and recovers naïve MCT if correlations are approximated as Gaussian. ABHT uses this heuristic comparison to identify a volume fraction above which activated processes are needed, $\phi = 0.432$. At lower volume fractions, the effective free energy is a monotonically decreasing function of the separation distance between particles, encouraging particles to move away from their neighbors, which they do relatively freely. Above $\phi = 0.432$, barriers in the energy landscape become sufficiently high that "activated processes" are required for particles to move relative to one another and explore other configurations. However, ABHT predicts *finite* relaxation time at $\phi = 0.58$, contradicting scaled MCT as well as experimental data forced to fit the inherently divergent VFT equation that assumes $\phi_g = 0.58$. Indeed, ABHT predicts that no divergence occurs for $\phi < 0.64$. In fact, a "best" fit to the data suggests no divergence even at random close packing[36]: the best fit grows markedly faster than theoretical data points and the latter suggest no divergent slowing of the relaxation time, at any volume fraction. More recently, ABHT has incorporated phenomenological modeling of relaxation dynamics beyond $\phi = 0.58$, which the authors hypothesize are collective. Physically, within a cage of nominal size $6a$ (for particles of radius a) particles are said to undergo non-vibrational hopping displacements and experience a local excitation strain field that allows the cage to expand, with the region outside the cage undergoing collective harmonic elastic motions to accommodate the local rearrangement within the cage[38,39]. These activated dynamics are hypothesized to drive cooperative motion that underlies the finite relaxation time. Other models for dynamics near the glass transition point include cage-growth models for hindered diffusion, which prescribe divergent behavior at maximum packing[81–87].

Overall, theoretical models advanced or adapted to explain the colloidal glass transition conflict with experimental observation: none predict diverging relaxation time at $\phi = 0.58$ and, further, the cooperative motion proposed by theory has yet to be observed in experiments. In particular, prescribing divergence anywhere (such as enforcement of the VFT, Krieger-Dougherty, or other *ad hoc* divergence model) is ill-advised, and the driving force for relaxation dynamics remains murky. Finally, all three theories (MCT, RFOT and ABHT) are equilibrium-based models and cannot address a key aspect of vitrification: aging. There has been an attempt in subsequent studies to detect dynamical heterogeneity as a signature of cooperative relaxation. For instance, Donati *et al.*[72] and Weeks *et al.*[73] observed dynamically distinct, durable strings or clusters of particles that emerged in the plateau of their mean-square displacement. Neither study reported relaxation within or of such structures, but they did hypothesize that they play some role in glassy behavior. One key breakdown in the literature ideas about cooperative motion as the mechanism for glassy relaxation is that experimental studies such as Weeks' suggest very small clusters of particles with length scales of two particle sizes, in contrast with theory such as RFOT which posits a divergent growth of cluster size as the glass transition is approached. We argue that the idea that cooperative motion drives relaxation is incomplete, because the detailed role of this motion is not explained. We recognize that in colloidal suspensions (whether in the dilute, liquid, or glassy state) the plateau between short-time self-diffusion and long-time self-diffusion by definition corresponds to correlated motion (see, e.g., Rallison and Hinch[88]). We believe that the role of such correlated motion is simply to relax a surrounding cage, permitting long-time self-diffusion to resume. Getting to the bottom of this, as well as identifying what role is actually played by such correlated motion, is one aim of the present study.

Medina-Noyola and co-workers have attempted to address aging in their non-equilibrium self-consistent generalized Langevin equation theory (NE-SCGLE)[40], based on a generalized Langevin equation[89] made self-consistent with a non-equilibrium extension of the Onsager theory of thermal fluctuations. NE-SCGLE predicts that a colloidal system can never reach thermodynamic equilibrium for volume fractions above $\phi = 0.582$, effectively portraying the glass transition as a crossover point below which the system can reach an intransient state but above which it cannot. This pioneering work addresses a key point rarely tackled directly in the literature: that intransient versus permanently transient dynamics may separate the liquid from the glass. No mechanistic picture is offered, however; what causes the transition from one regime to the other and how relaxation occurs at $\phi > 0.582$ are left unexplained. The theory predicts divergent growth of equilibration time (different than relaxation time), with divergence at $\phi = 0.582$. However, their companion simulations conflict: their systems suggest equilibration up to $\phi = 0.59$. Unfortunately, no simulations deeper into the glass region, ($\phi \geq 0.59$) are reported. While disagreement between theory and simulations, along with lack of a mechanistic model make the theory less convincing, NE-SCGLE provides important insights about the role of aging in diagnosing vitrification.

Aging behavior is one of the hallmarks of vitrified colloidal materials, as first demonstrated by the landmark experiments of Pusey and van Megen[29] that showed that colloidal crystallization can be delayed temporarily or indefinitely starting at volume fraction around $\phi = 0.60$. Their follow-on work[30,51,52,67] demonstrated the impact of aging on the de-correlation plateaux used to identify ϕ_g, a result subsequently overshadowed by the focus on the impact of size polydispersity[53,63–68] on ϕ_g. More recent return to the investigation of aging in experiments has called in to question once again whether there exists a divergently slow relaxation anywhere in volume fraction[90,91], a result that is key to the idea of whether an underlying thermodynamic colloidal glass transition exists. Further, it is known that in molecular glasses

mechanical "rejuvenation" leads to different responses than does thermal "rejuvenation"[92-94], and it is increasingly recognized in colloidal glasses[67,93,95,96] that sample preparation such as tumbling or shear melting[29,62,73,97] can shift the colloidal glass transition point by biasing structure and dynamics.

The theories reviewed above form powerful tools to describe several aspects of the colloidal glass transition phenomenon, and gave the community a set of consensus ideas that (a) cooperative relaxation of particles in finite-size domains enables decorrelated dynamics at $\phi > \phi_{g,MCT}$; (b) divergence of relaxation time occurs prior to random close packing, at $0.56 \leq \phi \leq 0.60$ (but this conclusion from modified MCT is contradicted by RFOT, ABHT and NE-SCGLE theories and recent experiments[53,98]), and an underlying thermodynamic glass transition exists (but this depends on fitting models that prescribe rather than predict divergence); (c) divergent growth of the size of cooperative relaxation regions makes particle motion over this length scale more and more difficult as ϕ increases; and (d) some activated process drives the cooperative relaxation. There remain fundamental issues with these consensus paradigms. Indeed, just the basic litmus test of the divergent relaxation time produces widely disparate results and requires *ad hoc* phenomenological approximation to locate it. Furthermore, the dynamical behavior close to jamming, either at the single-particle or collective scale, is virtually unexplored, even though dynamics are at the heart of decorrelation during the glass transition, thus a direct observation of cooperative motion deep in the glass is still lacking. Finally, theoretical modeling of vitrification kinetics and glassy aging are rarely considered except for a few phenomenological models[99-102], even though aging behavior has long been reported in the experimental literature. Overall, making progress seems to hinge on gaining access to particle-scale dynamics during and after the quench. Dynamic simulations can make a unique contribution to this effort.

In the present work, we combine large-scale dynamic simulations with experiments to carry out constant-volume, constant-number-density particle-size jumps from a colloidal liquid state to varying depths near and beyond the putative glass transition. Experimental realization of a similar protocol to trigger the glass transition was recently implemented with thermo-responsive microgel particles[103-107]; the first *in silico* modeling of a size-jump volume-fraction quench was implemented recently in our study of time-concentration superposition[108]. Here we expand that model to interrogate detailed particle-scale dynamics. Dynamic simulation is a powerful complement to experiments because of its ability to monitor individual particles to make detailed microscopic measurements such as coordination number, single-particle and collective dynamics, and contributions to osmotic pressure. Simulations are also free of many assumptions required by theory, e.g. they allow access to many-particle interactions, polydispersity and aging. Critically, we are free from the need to pre-suppose divergent (or any other scaling) of relaxation time, because we can perform quenches to arbitrarily close to maximum packing. By tracking particle dynamics as a function of age, we can infer directly the micro-mechanics of the relaxation process of a model colloidal system. To look closely at single- versus collective particle motion, we monitor colloidal dynamics via two means:
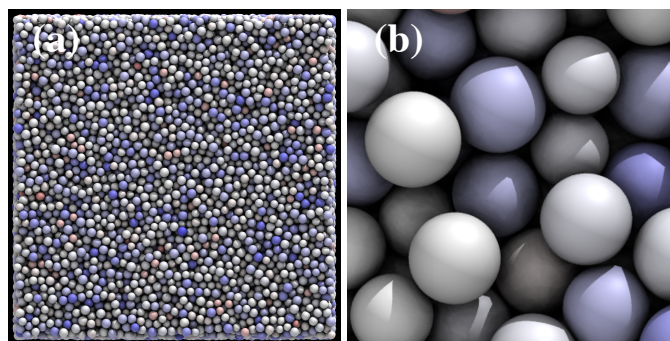

Fig. 1 (a) Snapshot of one periodic simulation cell at the final volume fraction $\phi_{\text{final}} = 0.63$. The color indicates the number of contacts of each particle; the color changes from red to white to blue as the number of contacts varies from 0 to 12. (b) $10\times$ magnification.

computing the decay of correlations via the intermediate scattering function and tracking particle displacements (to give mean-square displacement over time). In our companion experiments, particle dynamics are interrogated via the mean-square displacement as determined from the intensity autocorrelation function obtained in light scattering experiments.

The remainder of this paper is organized as follows: the study begins with presentation of the model system and methods in Section 2, including simulation techniques (in Section 2.1) and experimental setups (in Section 2.2). The results follow in Section 3. We first present results of self- vs coherent-intermediate scattering function in Section 3.1. We then focus on single-particle dynamics by comparing mean-square displacement and self-intermediate scattering function in Section 3.2. And finally we propose a new mechanism of glassy relaxation in Section 3.3. We conclude with a discussion in Section 4.

2 Methods

2.1 Simulation

The LAMMPS molecular dynamics package[109] provides an ideal platform due to its ability to partition particles over large domains across many processors, to enable parallel time-integration of particle positions and velocities within each domain. We build a system of 55,000 Brownian particles of size a suspended in a Newtonian solvent of density ρ and viscosity η, which is periodically replicated to model an infinite glass. A 7% size polydispersity mimics controlled experimental conditions. **Figure 1** shows a rendered image of one simulation cell as well as a magnified image showing the crowded structure of a colloidal glass at $\phi = 0.63$. Colloidal particles interact via hydrodynamic ($\boldsymbol{F}^H$), Brownian ($\boldsymbol{F}^B$), and interparticle ($\boldsymbol{F}^P$) forces, and the influence of these forces on particle motion is described by the Langevin equation, a stochastic force balance on each particle:

$$\boldsymbol{m} \cdot \left(\frac{d\boldsymbol{U}}{dt}\right) = \boldsymbol{F}^H + \boldsymbol{F}^B + \boldsymbol{F}^P. \tag{1}$$

Hydrodynamic interactions play a role in suspension mechanics even up to (and likely beyond) volume fractions as high as 0.55[110]. However, in the present work we make the simplify-

Soft Matter Accepted Manuscript

ing assumption that hydrodynamic interactions between particles can be neglected. The study of such freely-draining suspensions has led to many fundamental insights and results[111–114]. This is a reasonable approximation when the repulsion range between particles keeps their no-slip surfaces separated by at least 20% of the particle size. Thus the hydrodynamic force on each particle i moving with velocity U_i in a background flow with velocity $U^\infty(X_i)$ at the location X_i is of particle i determined by Stokes' drag law:

$$F_i^H = -6\pi\eta a_i [U_i - U^\infty(X_i)]. \qquad (2)$$

In this freely-draining limit, the Brownian force obeys Markovian statistics[115]:

$$\overline{F_i^B} = 0, \ \overline{F_i^B(0)F_i^B(t)} = 2kT(6\pi\eta a_i)I\delta(t), \qquad (3)$$

where I is the identity tensor and $\delta(t)$ is the Dirac delta distribution. The interparticle force is here modeled as derived from a spherically symmetric, steeply repulsive potential $V(r_{ij})$:

$$F_i^P = -\sum_j \frac{\partial V(r_{ij})}{\partial r_{ij}}\hat{r}_{ij}. \qquad (4)$$

Here, $\hat{r}_{ij} = r_{ij}/r_{ij}$, where $r_{ij} = X_i - X_j$ is the separation vector from the center of particle i to the center of particle j and $r_{ij} = |r_{ij}|$. In the present work we model colloids as nearly-hard spheres to correspond to experimental systems of hard spheres. Particle softness and permeability play a role in some colloidal glasses and modeling of these interactions requires additional parametrization of the interparticle potential, or even new approaches[116–127]. Soft glasses are an active and important area of study, where it has been shown that elastic deformation introduces a new relaxation mechanism[106,118,121–123]. Here we wish to focus on the most fundamental contributions to vitrification, entropic exclusion and Brownian motion, we focus on nearly-hard spheres, which we model via a nearly-hard-sphere Morse potential:

$$V(r_{ij}) = -V_0\left(2\exp\left(-\kappa[r_{ij} - (a_i + a_j)]\right) - \exp\left(-2\kappa[r_{ij} - (a_i + a_j)]\right)\right), \qquad (5)$$

giving the interaction between particles i and j with centers separated by a distance r_{ij}. The exponential shape provides steep repulsion to represent nearly hard spheres. In Equation 5, V_0 sets the depth of the potential well, κ^{-1} determines the well width, and a_i and a_j are radii of particle i and j, respectively. To represent a strictly repulsive interaction, we cut off the attractive part of the potential by setting the cutoff distance at exactly the minimum of the potential: beyond this distance, particles do not interact at all. We fix $V_0 = 6k_BT$ and $\kappa = 30a^{-1}$, which has been shown to recover the structure and dynamics of a hard-sphere suspension[9,10]. The novel feature of our model is that the glass transition is induced by changing both a_i and a_j as well as the cutoff distance, and this technique is crucial to forming a pristine glass, without the complicating effects of flow. Comparison of equilibrium structure, diffusion and osmotic pressure to published data[128–132] verifies that changes in particle hardness induced by the particle-size-jump algorithm are negligible. The particle velocities and positions are

advanced in time numerically using velocity Verlet integration[133] in LAMMPS. We select a small timestep, $\Delta t = 10^{-6}a^2/D$, for the integration, where a^2/D is the diffusive time required for a single particle of size a diffusing its size in a pure solvent, with the diffusion coefficient $D = kT/6\pi\eta a$. This gives a Stokes number small enough to faithfully model the colloidal (inertialess) physics. The small timestep permits very small overlaps that are then resolved via a standard Heyes-Melrose algorithm[134], where the entropic encounter contributes appropriately to the osmotic pressure.

Our computational studies comprise two parts. First, the system was "quenched" from a low volume fraction (liquid state) to a high volume fraction (solid state) by rapidly increasing the size of each particle at fixed system volume. In the present work, we fixed the initial volume fraction $\phi_{\text{initial}} = 0.50$ and the volume fraction quench rate $d\phi/dt = 0.25D/a^2$, and varied the final volume fraction between $0.56 \leq \phi_{\text{final}} \leq 0.63$. This flow-free method allowed us to transition from a liquid to a solid-like state without biasing the structural evolution. Second, after reaching the final volume fraction, we held the system at an iso-volume-fraction condition, letting it evolve under only Stokes drag, Brownian motion and entropic exclusion. During and following the quench, the positions, velocities, and particle-phase stress were tracked and utilized to characterize relaxation timescales and structural changes. Throughout volume fraction "quenches" and post-quench aging, we chose the diffusive time a^2/D to make all timescales t dimensionless in order to represent the relative rates of quench and aging with respect to Brownian motion, and we referred to the dimensionless time units as Brownian times, $t/(a^2/D)$. Thus, quenches in our simulations took place over a time interval $0.04 \leq t/(a^2/D) \leq 0.52$, much faster than the diffusive time of a bare particle so that structural relaxation during quenches was negligible. After each quench, the suspension evolved undisturbed to an age of $80,000a^2/D$, during which we monitored age-dependent structure and dynamics.

We track the absolute position $X(t)$ of each particle throughout the simulation. The mean-square displacement (MSD) is computed as

$$\text{MSD} \equiv \langle \Delta r(t)^2 \rangle = \langle (X'(t) - X'(0))^2 \rangle, \qquad (6)$$

where $X'(t) = X(t) - \langle X(t) \rangle$ and the angle bracket $\langle \cdot \rangle$ denotes an ensemble average over all particles. The coherent- and self-intermediate scattering function, $F(q,t)$ (CISF) and $F_s(q,t)$ (SISF) respectively, are computed as

$$F(q,t) = \frac{1}{N}\left\langle \sum_j \sum_k \exp\left[-i\mathbf{q}\cdot(X_j(t) - X_k(0))\right] \right\rangle_{\mathbf{q}\cdot\mathbf{q}=q^2}, \qquad (7)$$

$$F_s(q,t) = \frac{1}{N}\left\langle \sum_j \exp\left[-i\mathbf{q}\cdot(X_j(t) - X_j(0))\right] \right\rangle_{\mathbf{q}\cdot\mathbf{q}=q^2}, \qquad (8)$$

where N is the number of particles, $\mathbf{q}$ is all wavevectors of magnitude $q = 2\pi/L$, L is the specific length scale we want to probe, and X_j is the absolute position of particle j. The measurements of the MSD directly probe particle encounters that, at lower volume fractions, require traversal over long distance in order to sample many different configurations as it wanders through the suspen-

sion. The measurements of the CISF and the SISF, however, track decorrelation over one specific wave number, thus we expect that the two types of measurements may generate different results regarding length scales as well as timescales. The SISF takes on a value of unity when particle positions are strongly correlated, and a value of zero means that particle positions have completely decorrelated. If relative particle motion in a suspension is Brownian, the correlation in particle positions can decay from one to zero with a rate that depends on particle mobility, essentially distinguishing between a liquid state and a solid state.

Colloidal glasses exhibit at least two well-defined diffusive regimes, and these are typically interpreted as relaxation timescales. At short times, particles diffuse within a cage of nearest neighbors, producing the β-relaxation. At longer times, correlated interactions with the cage produce a plateau in both the MSD and the SISF. Emergence from the caging plateau indicates long-time self-diffusion, or α-relaxation. The α-relaxation time measured in MSD, $\tau_{\alpha,MSD}$, is obtained by fitting the MSD to the sum of two stretched exponentials as

$$\left\langle \Delta \mathbf{r}(t)^2 \right\rangle = A + B \left[1 - \exp\left(-(t/\tau_{\beta,MSD})^{p_1}\right) \right] \\ + C \left[1 - \exp\left(-(t/\tau_{\alpha,MSD})^{p_2}\right) \right] + Dt, \quad (9)$$

where A, B, C and D are fitting parameters. The stretched exponential requires $p_1 < 1$ and $p_2 < 1$. Equation 9 thus incorporates essential phenomenology for dense suspensions; the parameter D is related to the long-time self-diffusion coefficient D_∞^s by a 1/6 scaling factor, $D_\infty^s = D/6$. Similarly, the relaxation time measured by the SISF is obtained by fitting a double stretched exponential to the SISF:

$$F_s(q,t) = E \exp\left[-(t/\tau_{\beta,SISF})^{p_3}\right] + F \exp\left[-(t/\tau_{\alpha,SISF})^{p_4}\right]. \quad (10)$$

Here, E and F represent the magnitude of decorrelation for β-relaxation (from unity to the β-plateau) and α-relaxation (from β-plateau to zero), respectively. As such, their sum is unity. Both p_3 and p_4 are smaller than unity, and the α- and β-relaxation times are represented by $\tau_{\alpha,SISF}$ and $\tau_{\beta,SISF}$, respectively, extracted from Equation 10.

2.2 Experiment

We carried out experiments to compare with simulations, and here we describe the materials and methods. The colloidal samples are polystyrene-poly(N-isopropylacrylamide) (PS-PNIPAM) core-shell particles, with 18% polydispersity determined by dynamic light scattering[108]. The detailed synthesis process is discussed in our previous work[108]. We focus on a narrow temperature range between 27°C and 30°C, such that the size of PS-PNIPAM particles measured by dynamic light scattering depends linearly on the temperature and can be described by a linear fit $d_H(T) = 194.65 - 2.15T$, where d_H is the hydrodynamic particle diameter in nanometers and T is temperature in °C, although the accuracy of locating the no-slip surface on microgel particles is the subject of ongoing study. The experimental "effective" volume fraction is then calculated as $\phi_{eff}(T) = \phi_{collapsed}[d_H(T)/d_{collapsed}]^3$,

where $d_{collapsed}$ is the hydrodynamic particle diameter obtained from dynamic light scattering, in the collapsed state. Here, $\phi_{collapsed}$ is the volume fraction in the collapsed state, computed from the density and mass fraction of dry particles. The descriptor "effective" is meant to convey that the volume fraction in our experiments is calculated based on the hydrodynamic diameter of particles in dilute suspensions obtained via dynamic light scattering and does not account for particle deformation at high particle concentrations. The measured volume fraction of the collapsed state further introduces uncertainty to the true volume fraction of the particles[105,108,135–137]. As a result, we report "effective" volume fraction as a relative volume fraction comparing to a reference state (the collapsed state).

Because the microgel particles are thermo-responsive, cooling causes particle size to increase, triggering a volume fraction up-jump (quench), analogous to the process modeled in our simulations. To make consistent temporal comparison to our simulations, we normalized experimental timescales with the diffusive time of PS-PNIPAM particles, which was calculated as $a^2/D = 6\pi\eta a^3/kT \approx 0.01s$[108]. All volume fraction jumps took place over a time interval of 100 s, which corresponds to $\sim 10,000 a^2/D$. Following volume fraction jumps, the samples were aged up to $700,000 a^2/D$. The quench rate differs between experiments and simulations, which is expected to influence the dynamics of the young glass more than those of the aged glass. Because the relaxation time is calculated at very long times, the stronger effects of quench rate on system dynamics just after the quench is to some extent avoided, although it may introduce other lasting effects. The cuvette, which is used to seal the sample against moisture leakage, is mechanically compliant with the sample, meaning that the whole system is always in equilibrium with the ambient pressure, thus it is not a pressure cell and the change of temperature cannot cause a change in stress. As a result, thermal stresses can be neglected. Subsequent aging processes following the jumps were explored by dynamic light scattering experiments, performed using multi-speckle diffusive wave spectroscopy in backscattering geometry[138], in which the sample was illuminated by a 633 nm wavelength laser. A CCD camera with frame rate of 120 frames/s collected the scattered light, from which the intensity autocorrelation function $g_2(t)$ was obtained. The relaxation time in experiments was calculated as the time at which the intensity autocorrelation function $g_2(t)$ dropped by half of its initial value[103,104,106]. The intensity autocorrelation function $g_2(t)$ takes the following form related to the MSD[139]

$$g_2(t) - 1 = \exp\left[-2\gamma\sqrt{k_0^2 \langle \Delta \mathbf{r}(t)^2 \rangle + b} + 2\gamma\sqrt{b}\right] \quad (11)$$

where the parameters in the equation are taken from elsewhere[140]: $\gamma = 1.9$ is to quantify low-order scattering; $b = 0.0035$ characterizes the geometry; $k_0 = 2\pi\lambda/n$ is the wave number with $\lambda = 633$ nm and refractive index $n = 1.33$. The MSD in experiments was extracted from Equation 11 by solving for $\langle \Delta \mathbf{r}(t)^2 \rangle$, providing another basis of comparison to our simulations. The glass transition was identified as the effective volume fraction at which relaxation time exceeds $10s$.

2.3 Relating simulation to experiment

Our goal is improved understanding of the hard-sphere colloidal glass transition, without the complicating effects of particle deformation or flow. The ideal experimental system is one in which the concentration increase is triggered with no change in interparticle potential. While we aim to accomplish this by rapidly increasing the pressure of a hard-sphere system to compress the solvent, such experiments are still in development. To make progress, we use sudden swelling of microgel particles to increase volume fraction [103–107], but the swollen particles are substantially softer. Softness complicates the calculation of volume fraction and introduces elastic deformation and relaxation that shift the random close packing (and presumably the glass transition) point to higher volume fractions. Softness may also underlie finite relaxation time at very high volume fractions. Dynamic simulations are essential to dealing with such issues. The experiments thus serve to have established a set of tests and results that are postulated to originate from particle softness, and we perform these same tests on hard particles in simulations to disambiguate the effect of softness. As such, we isolated the effect of entropic exclusion and Brownian motion by starting with the simplest hard-sphere model. While previous studies of hard-sphere colloidal suspensions have used shear-melting in experiments [29,30,51,53,67,73,97,98] (which generate non-equilibrium structures that naturally lead to aging but are biased by external flow and are known to exhibit different behaviors from the structure obtained in volume fraction quenches [96]) and event-driven method in simulations [132,141] (which focus on "equilibrium" amorphous state and cannot model aging) to generate a dense, amorphous initial configuration, our previous work [108] and this study are the first to implement a nearly-hard-sphere particle-size jump in simulations to generate non-equilibrium configurations without inducing an external flow. Our algorithm is also a "true" volume fraction quench as it is free of the effect of temperature changes as induced in our experiments [142]. As a result, the comparison between hard-sphere simulations and soft-sphere experiments is qualitative: we do not and should not expect a quantitative agreement; rather, similarities and differences should lead to a better perception of what other experiments and what other simulations need to be done next to fundamentally understand the physical picture of the glass transition. This is discussed as future work.

3 Results and Discussion

To interrogate the hypotheses that collective motion produces glassy relaxation that grows divergently slow with high volume fraction, here we measure and compare both single-particle and collective dynamics via the self-intermediate scattering function (SISF) and the coherent intermediate scattering function (CISF), respectively. We also present measurements of the mean-square displacement (MSD) as a complement to the SISF. These results are followed by analysis of the volume-fraction dependence of the relaxation time, leading to a new mechanistic model for relaxation.

3.1 Effect of collective dynamics

We quench the system from a colloidal fluid into the putative glass region, from $\phi_{\text{initial}} = 0.50$ to sequentially deeper quenches: $\phi_{\text{final}} = 0.56, 0.57, 0.58, 0.585, 0.59$, and 0.595, using the method described in §2. Following each quench, we allowed the system to age to an intransient state where dynamics no longer change in time. The coherent and self-intermediate scattering functions, CISF and SISF respectively, were measured at each volume fraction and are plotted in **Figure 2**. Four plots are shown, one each for scattering wave numbers $qa = 3.25$, $qa = 1.57$, $qa = 1$, and $qa = 0.5$ corresponding to correlated dynamics over a length scale approximately equal to 2, 4, 6, and 12 particle radii, respectively. Physically, the SISF describes single-particle diffusion over the length scale $L \sim 2\pi/qa$, while the CISF represents collective dynamics of a particle "cluster" of size $L \sim 2\pi/qa$. By definition the CISF includes a "self" part (the SISF) and a "distinct" part; the magnitude and rate of decay of the CISF relative to those of the SISF reveals how important collective dynamics are, relative to self-motion. The rate of decay is typically the focus of analysis in the literature; thus it is typical to normalize the CISF on its initial value (the qa-dependent static structure factor, SSF) and observe their relative rates of decay from unity (the initial value of the SISF is always unity). The earliest time shown on the log-linear plot is at $0.04a^2D$.

At $qa = 3.25$, the rate of decay of the CISF and SISF are the same, which is expected, since both measure the motion of a single particle moving its size. There is a nearly instantaneous decorrelation at very short times followed by slower decay that becomes a plateau at high volume fraction, and finally a long-time decay emerges. However, over longer length scales of several particle sizes [**(b)-(d)**], the CISF tracks the abundance of the structures of those length scales and how the coherence of such structures relaxes. The CISF gives a measure of how a collective structure decorrelates from its initial configuration. When this structure involves only one particle, the decorrelation is the same as the SISF [**(a)**]. When two or more particles are involved [**(b)-(d)**], there is a more substantial early-time decorrelation; for example two particles quickly diffuse into a new pair configuration. When more particles are present, it takes longer for this initial reconfiguration to occur, as shown by the monotonic growth of the early-time relaxation with decreasing wavenumber. Nonetheless, for $qa \leq 2$, the early-time nearly-instantaneous drop in the CISF is more pronounced than the SISF, indicating that even though each particle has not moved far from its original position (SISF), the correlation of dynamics across different particles (CISF) is already weak. Thus the short-time collective dynamics of a set of particles decorrelate faster than the self motion of particles at short times, meaning that the short-time relaxation is dominated by the slower process, that is, the self motion. At intermediate times the CISF and the SISF both enter a glassy plateau at around the same time. This correlated motion has well-known meaning in the SISF, indicating that the motion of an individual particle is hindered by its neighbors as it attempts to escape its surrounding cage. The meaning of the CISF in the glassy plateau may reflect how the surrounding cage relaxes. We remark on the mag-

nitude of the CISF relative to the SISF. Recall that normalization can mask the relative magnitude of the CISF and the SISF. For small wave numbers $qa \leq 2$ in our purely repulsive, nearly hard-sphere system, the Static Structure Factor is small (~ 0.04), thus the un-normalized CISF is two orders of magnitude smaller than the SISF. Overall this suggests that cooperative motion may play a role in cage "melting" during the plateau, but self-motion seems to be the primary mechanism for reconfiguration of the cage. At long times, the curves merge and decay together toward zero, which is expected: as each particle has moved far enough to decorrelate from its original position, the surrounding structure of the suspension also changes. The CISF seems to persist as long as the SISF deep into the glass at $\phi \geq 0.585$, but taking into account the very small static structure factor (~ 0.04) at $qa \leq 2$ normalizing the CISF, the contribution of collective motion to decorrelation is much smaller than that of self-motion. Our results contradict the proposal in prior theories[28,35,36,38,71,76] that collective motion is the activated process that permits relaxation beyond $\phi_{g,MCT}$ but diverges as collective motion must occur over larger and larger domains; we find evidence that no such structural domains exist. The cooperative-relaxation model was additionally problematic because it stopped short of describing how such motion actually contributes to finite relaxation time. Our results suggest that correlated motion, which is distinct from collective motion[88], plays a

weak role in melting the glassy plateau. In the simplified model of a cage of particles that opens and permits one to escape, the trajectories of the particles are correlated but certainly not aligned. These results suggest that there are no appreciable dynamics for structures larger than a particle size, and that long-time relaxation occurs via self-diffusion. In the next section we turn our focus to self-motion.

3.2 Single-particle dynamics: decorrelation and diffusion

Now having eliminated large-scale collective motion as a primary mechanism for glassy relaxation, we focus our attention on self motion, the SISF. In most experiments, the SISF is plotted for only a single wave number, $qa = 3.25$, which probes decorrelation only over a single length scale. But dense suspensions exhibit relaxation over many length scales, which cannot be revealed by the single-wave number SISF. As shown in **Figure 2**, one way to evaluate relaxation over other length scales is to measure the SISF at many different wave numbers or, alternatively, one can measure particle displacements directly and compute the mean-square displacement (MSD). The key mechanistic behaviors being sought are (a) does long-time self-diffusion continue, and (b) what sort of motion (activated process) "melts" the glassy plateau beyond $\phi_{g,MCT}$, permitting long-time self-diffusion to continue?

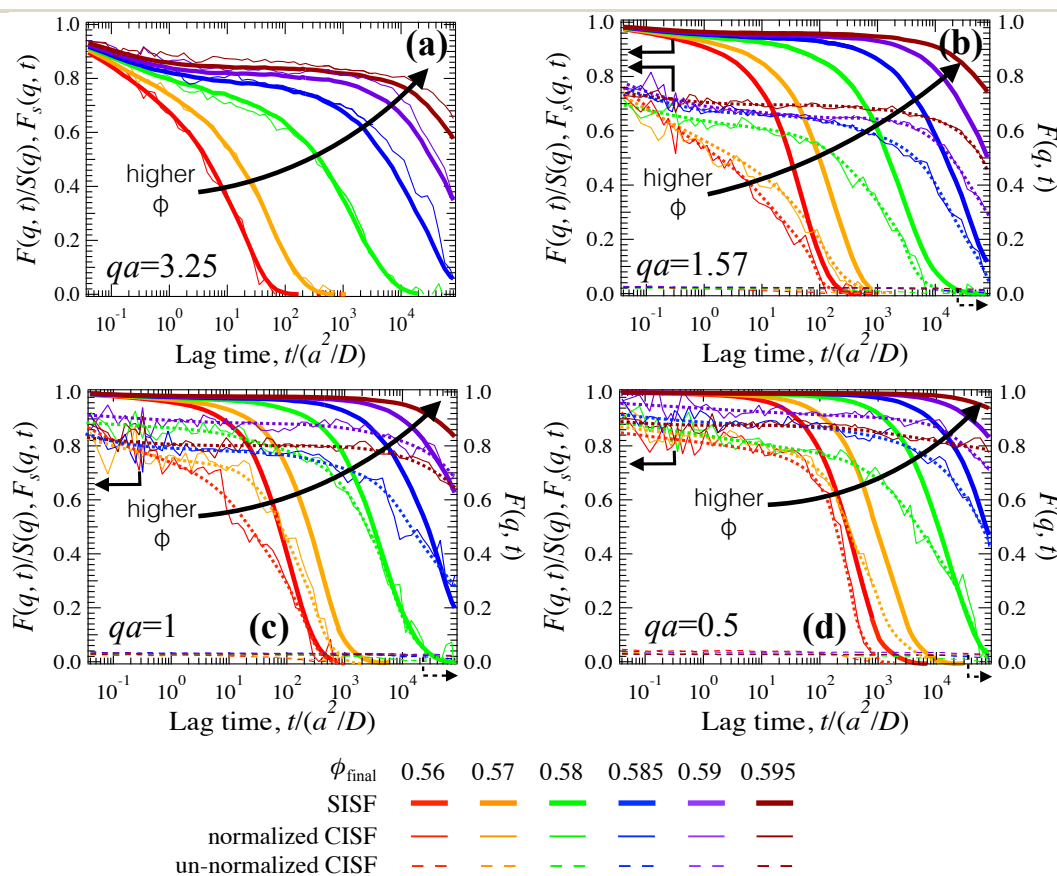Since we will compare post-quench particle dynamics via two

Fig. 2 SISF and CISF at $qa = 2, 1$ and 0.5 for quenches near to the glass transition at $0.56 \leq \phi \leq 0.595$. The SISF is plotted as thick solid lines, and the CISF normalized by its initial value (the static structure factor) is represented as thin solid lines; these two curves are plotted against the left axis. The un-normalized CISF is plotted as dashed lines on the right axis. The dotted lines are a guide to the eye for the normalized CISF.
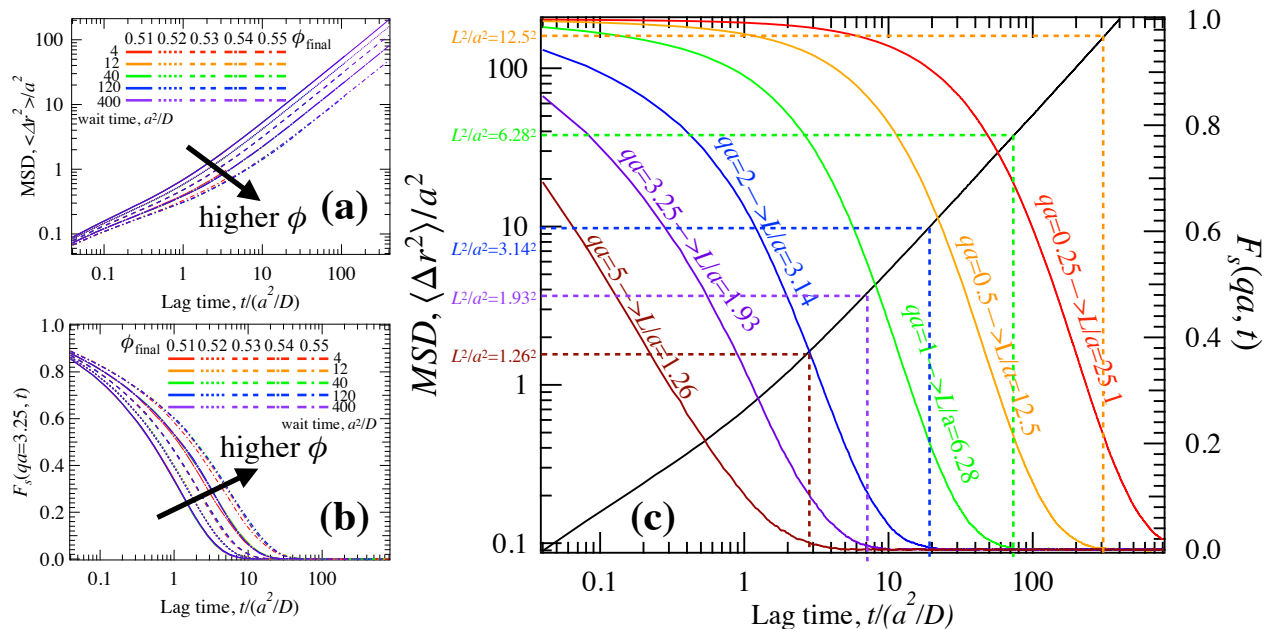
Fig. 3 Diffusion and decorrelation in (supercooled) liquid region. (a) Mean-square displacement as a function of lag time at different wait times for volume fraction jumps from $\phi_{initial} = 0.50$ to different final volume fractions (indicated by the arrow) within the range of 0.51-0.55, from top to bottom. (b) Self-intermediate scattering function vs lag time at different wait times for the same range of volume fractions (indicated by the arrow) of 0.51-0.55, from left to right. Curves at different wait times after the jump ($4a^2/D$, $12a^2/D$, $40a^2/D$, $120a^2/D$, and $400a^2/D$) are almost indistinguishable, as different colors indicating different wait times (shown in the legend) overlap with each other. (c) Mean-square displacement (black solid line) and self-intermediate scattering function at different wave numbers (indicated by the colored text on each curve) as a function of lag time, at $\phi = 0.51$. The colored dashed lines are snapshots of the MSD that correspond to length scale interrogated by each wave number.

measurements, MSD and SISF, we first frame the comparison in a thermodynamically well-defined transition: a jump from a low concentration liquid state to a higher concentration, still liquid state. We execute jumps from $\phi_{initial} = 0.50$ to sequentially deeper quenches: 0.51, 0.52, 0.53, 0.54, and 0.55. We expect these systems to be in the supercooled liquid region[2]. **Figure 3(a)** shows the MSD plotted as a function of lag time for all of these quenches; the measurement was taken at several different values of wait time after the quench. Below $\phi = 0.53$, the curves for each volume fraction are indistinguishable, which signifies a lack of aging, indicating that the reorganization of the initial structure of the fluid introduced by the rapid concentration change is nearly instantaneous. As expected, the MSD shows barely-visible plateaux and long-time dynamics remain diffusive. For $\phi \geq 0.54$, the MSD curve at the earliest wait time (red, wait time=$4a^2/D$) is separated from the other curves (ages), suggesting that a finite but short time is needed for the system to relax. However, the system reaches an intransient state at finite times where particle motions completely decorrelate, demonstrating that the system is in the supercooled liquid state, which is not far from equilibrium, and thus the measurements in this terminal state are unambiguous. In **Figure 3(b)**, the SISF for the same systems and the same quenches are plotted for $qa = 3.25$, demonstrating behaviors very similar to that of **Figure 3(a)** for the MSD. We recall that $qa = 3.25$ corresponds to α relaxation over a length scale of about one particle diameter, in contrast to the MSD plot which shows relaxation over many length scales. Because particles can diffuse far beyond one particle size in the supercooled liquid state, the MSD and

the SISF can access the same timescales and length scales. To illustrate this point, **Figure 3(c)** gives a physically intuitive connection between the MSD and the SISF at various values of wave numbers qa for $\phi = 0.51$. The black curve is the MSD, and the colored curves are the SISF at several wave numbers as indicated by the adjoining colored text. The time required for the MSD to reach the length scales probed by the SISF are exactly the same as the time required for the corresponding SISF to decay to zero. Thus, in the supercooled liquid region, the MSD and the SISF measurements are equivalent: the SISF can be mapped exactly to the particle diffusion by probing multiple length scales, which reflects the physical long-time self-diffusion, which occurs via migration from one local "cage" of nearest neighbors to another and another. That is, in a dense suspension of mobile particles, diffusive decorrelation requires long-distance motion throughout the suspension to encounter numerous configurations. The fact that the MSD and SISF at $qa = 3.25$ give the same answer indicates that the "cage" size and particle size are the same in the supercooled region. We next ask if this equivalency holds at higher volume fractions.

Upon quenching to higher volume fractions, the MSD and SISF both now exhibit important new behaviors: the emergence of a glassy plateau and long-time dynamics that emerge only after a transient phase. These non-equilibrium behaviors indicate the start of the glass transition. We recall that in **Figure 3**, a system quenched into the liquid region relaxes very quickly from its initial state following the quench, but now at higher volume fraction, particle dynamics change with time following the end of the
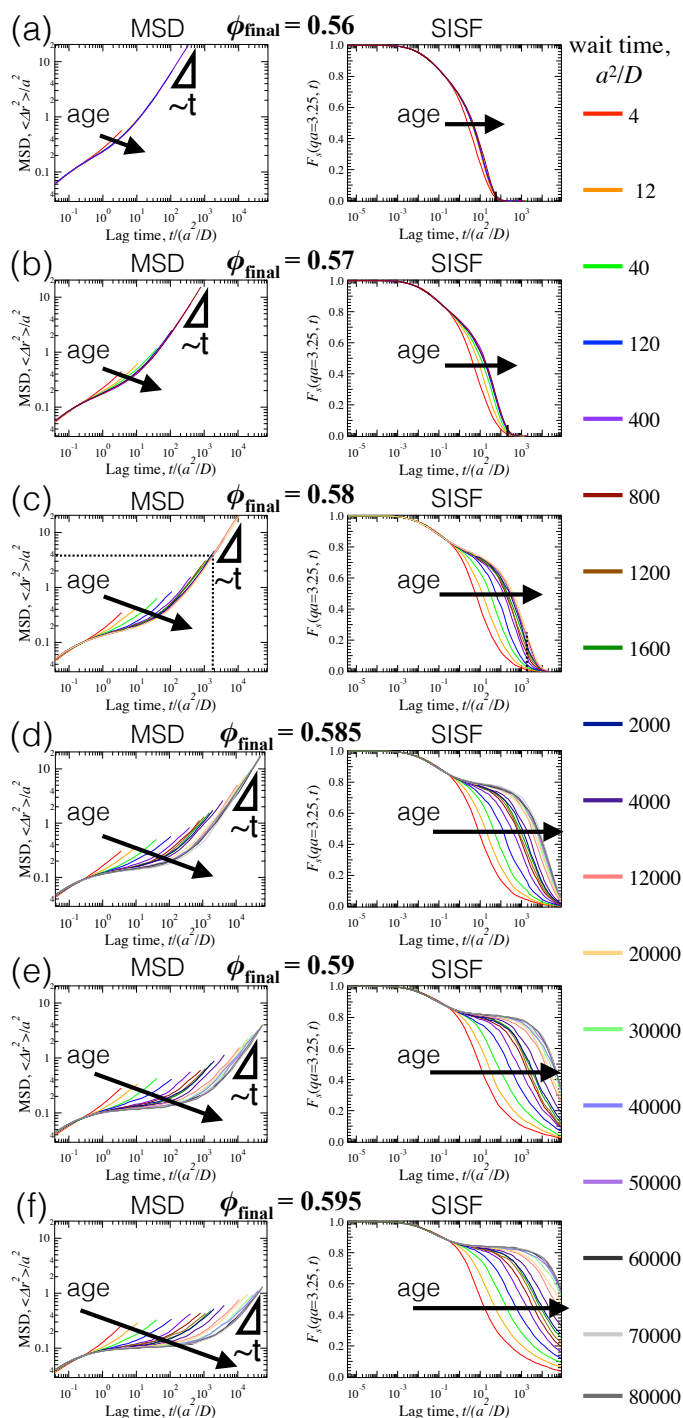
Fig. 4 MSD and SISF near to the glass transition: how they differ and age effects. (a)-(f) Simulations comparing MSD to SISF for $\phi_{\text{final}} = 0.56, 0.57, 0.58, 0.585, 0.59, 0.595$ from top to bottom, all quenched from $\phi_{\text{initial}} = 0.50$. Colors indicate different wait times, shown in the legend. In contrast to Figure 3, decorrelation changes with age (wait time), taking longer as the sample gets older.

quench – the curves separate. This is illustrated in **Figures 4(a-f)**, which shows six side-by-side plots of the MSD and the SISF corresponding to six different quenches. Each plot gives decorrelation versus lag time, and several curves in each individual plot represent different wait times (ages) after the volume fraction quench

(at which the lag-time measurement was begun). Progressively deeper quenches are shown sequentially in panels (a) through (f), all having started from the liquid state $\phi_{\text{initial}} = 0.50$. The final quenched volume fraction ranges from $0.56 \leq \phi_{final} \leq 0.595$. At *early* lag times, both MSD and SISF exhibit decorrelation: the MSD is linear and the SISF shows characteristic β relaxation. That is, both the MSD and SISF reveal short-time self diffusion. For both the MSD and the SISF, the early-lag time diffusivity is independent of age (wait time). The mechanistic origin of this age-independent diffusion is the small length scales involved: short-time particle dynamics take place over length scales much too small to disturb surrounding structure, and thus require no structural relaxation to decorrelate. This is so-called in-cage diffusion. At *intermediate* lag times, a plateau emerges in both the MSD and the SISF, revealing the particles' attempt to migrate out of their nearest-neighbor cages, which produces correlated motion. The plateau takes time (age) to emerge: just after the jump, relaxation is rapid and surrounding cages are evidently liquidlike. But as vitrification continues with age (wait time), cages apparently "firm up", requiring aging in order for particle motions to decorrelate. This characteristic caging plateau reflects motion of particles attempting to squeeze out of a local cage — a cage that gets more durable with age (wait time). The lengthening of the plateaux with age becomes more and more pronounced with deeper quenches. Notably, the vertical overlap of the plateaux suggest that the "cage" size is set by volume fraction, and does not change with age. At *long* lag times, the curves peel apart as they exit the glassy plateau both for the MSD and the SISF, indicating that particle dynamics slow down with age. But eventually the curves rejoin onto an overlapping single curve at long times, signaling the emergence of a long-time intransient state. It is important to wait "long enough" to let the glass age to an intransient state prior to drawing conclusions about terminal behavior. Now that we are able to observe the terminal behavior in the volume fraction range ($0.56 \leq \phi \leq 0.595$), we first focus on the mean-square displacement: the MSD becomes linear again for all volume fractions studied which, for 7% polydispersity, is well into the glass [52,67]. This result signals finite relaxation time within the putative glassy state, in contrast to prior predictions [30,51,77]. In fact, the dynamics remain diffusive up to $\phi = 0.59$ and nearly diffusive even up to $\phi = 0.595$ after a long plateau, suggesting that correlated motion eventually liberates particles from the caging plateau to let them undergo long-time self-diffusion to relax the structure to the intransient state. That is, long-time self-diffusion is not only the "signal", it is also the mechanism of glassy relaxation.

Our experiments confirm via dynamic light scattering the dynamical slowing down with age, shown in **Figure 5**, where a similar lengthening plateau emerges with increasing wait time, although the plateaux do not overlap, possibly due to the limited time window that can be accessed in the experiments. Yet the particle dynamics also display a nearly diffusive long-time regime for all effective volume fractions explored in our experiments , resembling our simulations (as a reference, the nominal glass transition in our experiments, defined as the effective volume fraction where relaxation time exceeds 10 s, is at $\phi_{\text{eff}} = 0.390$).
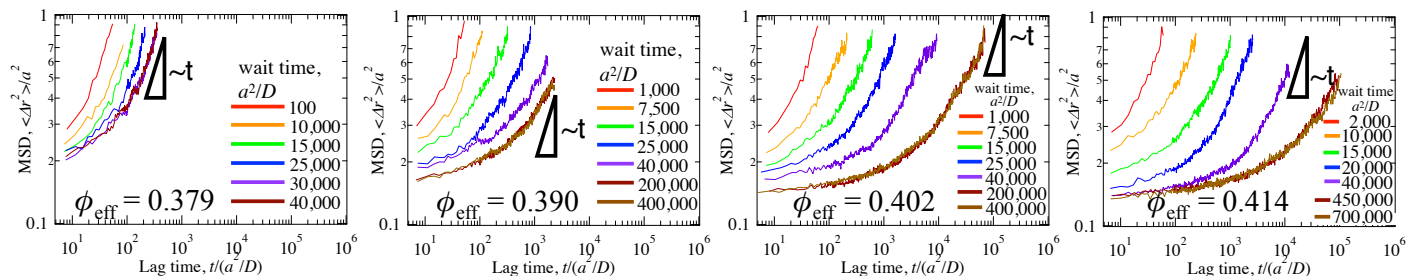
Fig. 5 Experiments showing MSD from dynamic light scattering, all quenched from $\phi_{\mathrm{eff}} = 0.364$, measured at different wait times as it evolves into an intransient state. Aging slows relaxation, but the duration of the quench obscures early-time behavior.

However, returning to simulation data reveals a breakdown in the agreement between the MSD and SISF also emerges in the glass: decorrelation takes much longer for the SISF than for the MSD at a given quench depth. We demonstrate this discrepancy in **Figure 4(c)** at $\phi = 0.58$ by performing the same test as **Figure 3**. We recall that the SISF probes decorrelation at $qa = 3.25$, corresponding to a length $L/a = 1.93$. The corresponding mean-square displacement, $\langle \Delta r^2 \rangle / a^2 = 1.93^2$, is obtained at $t \sim 1,900 a^2/D$, marked as a vertical dashed line in the same plot. However, by that same time, $F_s(t = 1,900 a^2/D) \approx 0.25$, which means that particle dynamics over the length scale of $qa = 3.25$ are still significantly correlated. Thus the MSD shows diffusive behavior but the SISF does not. This decoupling of the MSD and the SISF starts as low as $\phi = 0.56$ and is present up to at least $\phi = 0.595$. Prior studies have reported a breakdown in the Stokes-Einstein relation, termed a decoupling of mean-square displacement from viscosity (relaxation time) [143–145] and in some cases predict that total breakdown will occur in the glass when length scales grow divergently large [146]. However, our interpretation and mechanistic explanation are not related to the prior phenomenology described: the breakdown of the equivalency between the MSD and the SISF reported here pertains to the hindrance of a cage-escape process. We report a decoupling of the cage size from the particle size — which can be discovered and quantified only via the analysis of multiple wave numbers of the SISF; this is discussed next.

The contrast of this decoupling behavior to the exact match between the MSD and the SISF in the liquid region shown in **Figure 3** suggests that the two methods probe different length scales in glassy suspensions. The long-time MSD measures relaxation associated with a length scale set by *a cage size*, and these dynamics are reflected by the caging plateau, i.e. the length scale associated with the plateau height. As the volume fraction increases, cages become tighter. Thus, the MSD probes not only relaxation, but also reveals that the characteristic length scale over which it occurs changes with volume fraction. In contrast, when the SISF is measured at a fixed wave number for all volume fractions (at $qa = 3.25$, the typical value probed in experiments, which always probes decorrelations over the length scale of *one particle size*), it smears out this change in dynamics. Hence, the difference in the glassy region between the decorrelation times in the MSD and the SISF suggests that the wave number $qa = 3.25$ no longer represents the motion over a single cage, but rather measures relaxation over several cages. We then ask whether a different wave

number for the SISF would reconcile the two measurements, that is, if the relaxation of the SISF over the "cage" size matches the relaxation of the MSD.

To this end, we repeated the measurement of the SISF decorrelation for several values of qa, for $\phi_{final} = 0.58$ and plotted the results in **Figure 6**. The most revealing result is that the relaxation of the SISF at the wave number $qa = 10$, which is comparable to the length scale probed by the plateau of the MSD (much smaller than the size probed by $qa = 3.25 \sim$ particle size), is about an order of magnitude faster than the relaxation at $qa = 3.25$, which resolves exactly the difference between the relaxation times measured in the MSD and the SISF probed at $qa = 3.25$ in **Figure 4(c)**. The two measurement methods — MSD and SISF — now agree, and both suggest that in the glass, the "cage" size that sets decorrelation time is markedly smaller than a particle size. We can now recognize that the SISF taken at $qa = 3.25$ in a glass actually measures relaxation over several cages, explaining why decorrelation takes much longer than the MSD – and explains why the SISF measured only at one wave number can fail to recover ongoing diffusive relaxation captured by the MSD. We conclude that the mean-square displacement gives a sensitive measure, in the intransient regime, of the self-diffusion length and time scales underlying relaxation during aging in a colloidal glass, and this
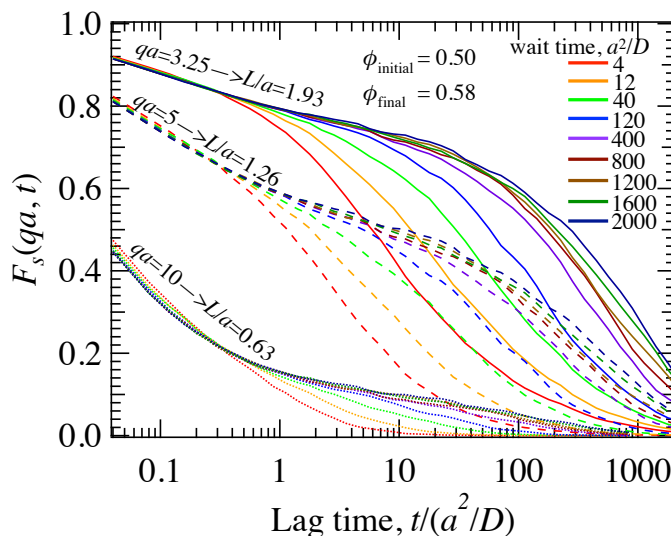

Fig. 6 The SISF for $qa = 3.25, 5$ and 10 from top to bottom at $\phi_{\mathrm{final}} = 0.58$.

length scale decreases with increasing volume fraction as the putative glass transition region is traversed.

Overall, our results suggest that glassy relaxation is a two-step process of cage melting via correlated (but not collective) motion, followed by long-time self-diffusion that relaxes the glass into the intransient state. The fact that the decoupling between the MSD and the SISF emerges at the onset of aging dynamics, i.e. around the putative glass transition at $\phi \approx 0.56$ where long-range motion is suppressed, suggests a change in the mode of self-diffusion. We discuss this next.

3.3 "Dense diffusion" as a mechanism of glassy relaxation

The key results thus far are that both the MSD and SISF confirm that self-diffusive dynamics emerge well into the glass and act to relax the glass toward the intransient state; and that this long-time self-diffusion in a colloidal glass occurs over very short length scales – much smaller than a particle size. This contrasts with the long-distance motion required in familiar models of long-time self-diffusion, where cage-to-cage migration enables long-time decorrelation over long distances required for particles to explore many other configurations[81,82,87,88]. Those prior theories of long-time self-diffusion have focused on the contact value of the radial distribution function, $g(2)$, that grows with volume fraction, suggesting that the cage size grows and the long-time diffusion becomes cooperative as it involves more and more particles. This is in contrast to what we have already shown: that the emergence of long-time *self*-diffusion is facilitated by a lengthy correlated motion, both of which occur at a length scale only a fraction of one particle size. The key idea to preserve is the exploration of many configurations essential to decorrelation; in the intransient state, the system must sample sufficiently many configurations to decorrelate from its original state. However, our dynamical data show that the configuration sampling process happens over a length scale much smaller than one particle size. The question then becomes, how does it encounter sufficiently numerous configurations within a very small volume for its motion to decorrelate?

We propose that this small-scale long-time motion is actually the emergence of a "dense diffusion" regime representing a distinct form of long-time self-diffusion. Recall that the long-time self-diffusion is an ergodicity-restoring process where particles lose memory of past configurations. In suspensions with volume fractions far below maximum packing, all particles explore many different local arrangements by undergoing a random-walk process over long distances. At lower volume fraction there is significant space between the particles, facilitating this exploration; for this same reason they must wander long distances to decorrelate their motion, because there is a dilute configurational space (**Figure 7** top row). Over short length scales, a particle essentially samples only the solvent (i.e. no particle configurations are sampled); only over longer distances, when particles develop correlated motion as shown in the caging plateaux in the MSD, can they recognize a cage, and beyond this distance particle motion decorrelates and long-time self-diffusion emerges. As concentration increases, this plateau becomes more pronounced. Thus,

long-time self-diffusion is typically viewed as long-range motion, and it is ergodic: the configurations surrounding each particle are on average the same as the configurations probed by a tracer particle exchanging positions with other particles over long distances.

However, in very dense suspensions near to the glassy state, particles are constrained in tight structures. The dense region around a tracer particle creates a dense configurational space as well. Even though particles are restricted to a small volume and cannot trade places with others, now small movements of the neighboring particles around a tracer generate numerous different configurations; combined with its own small movements, the tracer particle can encounter these many configurations (**Figure 7** bottom row). The neighboring particles of the nearest neighbors undergo the same small motion, essentially cascading configurations far away to the tracer particle. Thus, instead of the surrounding cage melting and letting the tracer particle wander out, the tracer's motion decorrelates as it moves within its original cage, which deforms into entirely new configurations. That is, the cage deformation process is caused by all further surrounding particles cascading very small-scale relaxations to their neighbors and eventually to the tracer particle. In this way, the tracer samples the entire suspension wandering a small fraction of its own size.

The contrast between the two configurational sampling mechanisms can now be distinguished via comparison of **Figure 3(a)** with **Figure 4**. In supercooled liquids (**Figure 3**), particles can travel much farther than a particle size — even infinitely far — the familiar cage-to-cage migration in mobile dispersions. In contrast, in very dense suspensions (**Figure 4**) particles enter the long-time regime over a length scale much less than the particle size, showing that each particle is confined within the volume of its original cage, but the configuration of the cage has rearranged so substantially that the particle sees a different configuration. Without moving far beyond its original position in an absolute sense, each particle loses memory of its original cage. We highlight the fact that this is long-time self-diffusion of particles liberated by short-ranged correlated motion that relaxes the cage, rather than short-time self-diffusion as claimed in e.g. van Megen *et al.*[52].

This mechanistic model sheds new light on the colloidal glass transition. We view the glass transition as a region in volume fraction rather than a divergence point. Glassy arrest commences at around $\phi = 0.56$ where glassy aging emerges, but relaxation via robust self-diffusion continues, and takes place over the particle length scale (as evidenced by the equivalence of $S(qa = 3.25)$ and the MSD). "Deep arrest" follows at around $\phi = 0.58$, where long-time self-diffusion transitions from long-distance to "dense configuration", short-distance diffusion, over length scales much smaller than a particle size (as evidenced by the decoupling of $S(qa)$ and MSD), and structural relaxation continues. This long-time, short-distance self-diffusion remains well-separated (by a long, glassy plateau) from short-time self-diffusion. Complete arrest must then correspond to complete suppression of this dense diffusion. Whether this complete arrest is the same as the "zero temperature" vanishing of short-time self-diffusion remains to be
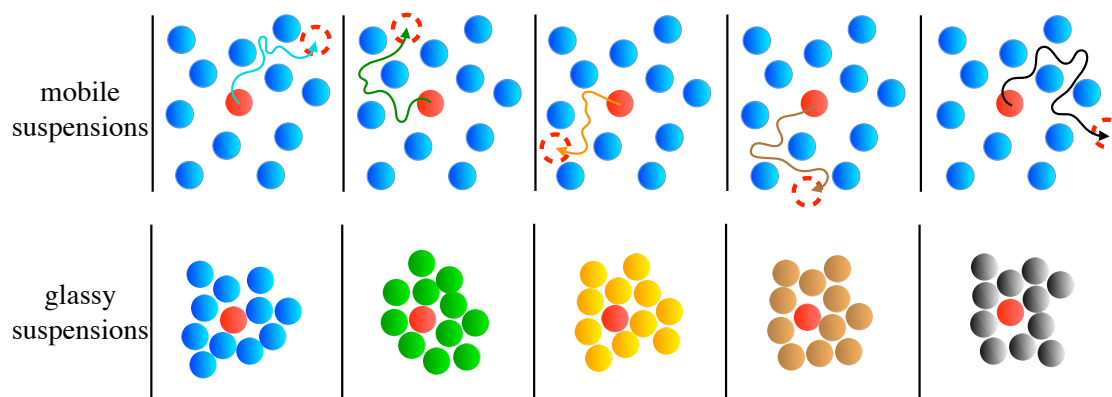
Fig. 7 Different mechanisms of sampling configurations. In mobile suspensions (top row), the tracer particle (red filled circle) wanders far from its initial position, undergoing long-time as well as long-distance self diffusion, to explore new configurations. Different colors indicate different paths the tracer particle can take, and each path ends up in a different configuration. In glassy suspensions (bottom row), the bath is so dense that the tracer particle (red filled circle) is restricted, and it can only move by small amount. However, new configurations are still formed by such small arrangements of many particles. The schematic shows that the tracer particle is surrounded by the same group of neighboring particles, but different colors indicate that the neighboring particles can form different configurations by undergoing long-time, but small-scale, self diffusion.
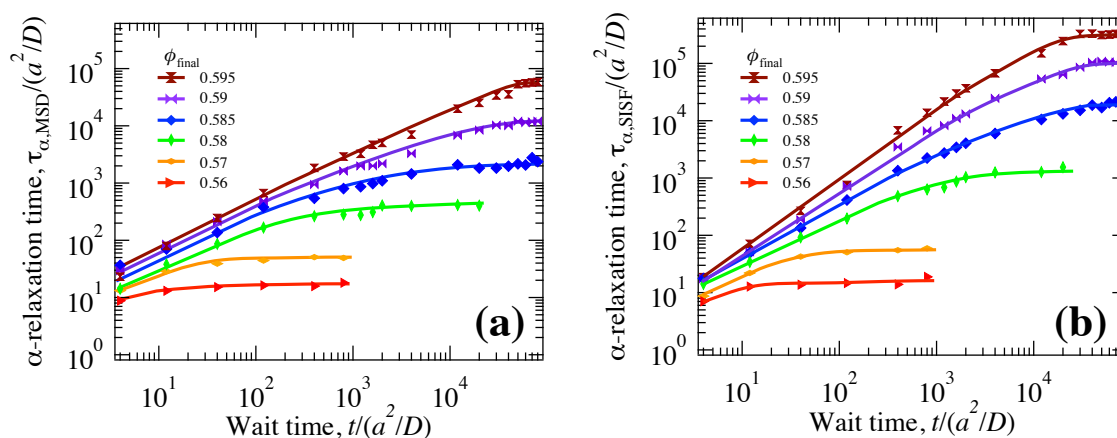

Fig. 8 Relaxation time vs age. (a) Relaxation time in simulation calculated from the MSD. (b) Relaxation time in simulation calculated from the SISF.

determined. We infer that only a strict topological constraint will fully eliminate such dynamics, i.e. at random close packing, analogous to the absolute zero temperature in a molecular glass.

Our proposed mechanism suggests that relaxation time —how long it takes for long-time diffusive dynamics (decorrelation) to emerge — remains finite in a colloidal glass. One way to measure the relaxation time is to fit the MSD data to Equation 9 or to fit the SISF data to Equation 10. However, as is clear in **Figure 4**, there are multiple curves for each final volume fraction owing to glassy aging. The standard approach is to let the glass age to an "intransient" state, where the MSD or SISF curves start to overlay one another, i.e., dynamics no longer change appreciably with age. It is perhaps an oxymoron to call a glassy state an intransient state, but the basic idea of measuring dynamics when they do not change appreciably seems like a good idea. In simulations we allowed the glasses to age for a time sufficiently long that the long-time MSD and SISF curves overlap, indicating attainment of an intransient state, up to $\phi = 0.595$ (cf **Figure 4**. These intransient data curves were fit at each volume fraction to Equation 9 (direct evaluation of the slope of the MSD curves produced identical results) and Equation 10 to give the the α-relaxation time,

τ_α. **Figure 8(a)** gives a plot of $\tau_{\alpha,MSD}$ and **Figure 8(b)** gives a plot of $\tau_{\alpha,SISF}$, versus the wait time. The results from all six quenches are shown in the plots. In both (a) and (b), the relaxation time grows with time as the glass ages into deep arrest, but for all quenches, each curve levels off to a plateau. The plateau relaxation time is the terminal value which can then be employed as an unambiguous measurement to test the idea of divergence.

In most prior approaches, the divergence of colloidal relaxation time is assumed *a priori*, using *ad hoc* extrapolations of the relaxation time to extend from moderate to high volume fraction, e.g. the Krieger-Dougherty equation[21] or the Vogel-Fulcher-Tammann fit[15–17]. These fits produce divergent behavior by construction, which then permits extraction of the precise volume fraction at which mathematical divergence takes place. Finding a divergent fit is frequently invoked to declare the existence of an "ideal" glass transition[71,77,147], but this logic is circular because the origin of the fits used to obtain divergence are built on an assumption that an ideal glass transition exists. By analogue with the molecular glass theory where the ideal glass transition is described as divergent relaxation times at the Kauzmann temperature being above absolute zero, $T_K > 0$, an ideal colloidal glass transition is simi-
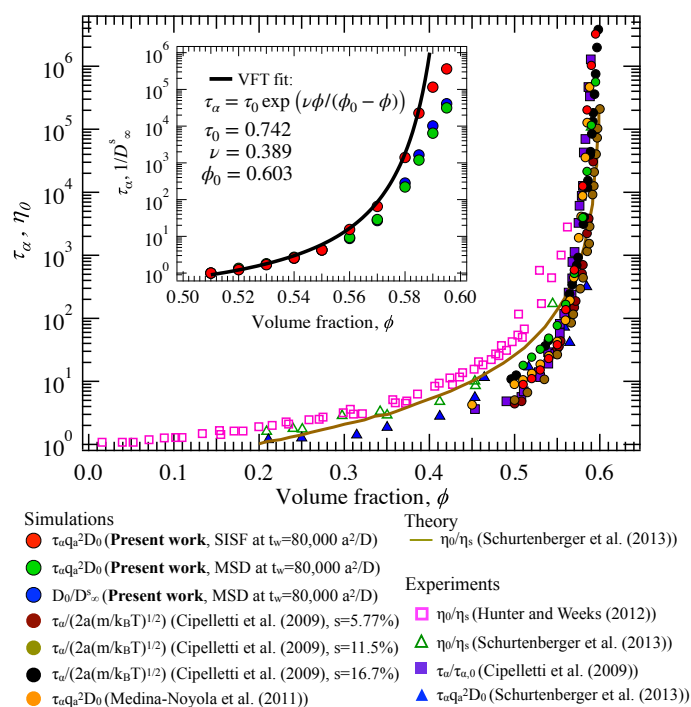
Fig. 9 Relaxation time measured from the MSD and the SISF as a function of volume fractions in hard-sphere simulations compared with literature. The detailed normalization for each measurement is indicated in the legend. The volume fraction represented here is the final volume fraction of each jump. Inset: relaxation time measured from the MSD and the SISF for $0.51 \leq \phi \leq 0.60$; each set of data is normalized to the value at $\phi = 0.51$ to collapse the data there for easy comparison. Black solid line in the inset is the VFT fit to relaxation time measured from the SISF; the fitting parameters shown are for the raw data of the SISF in the main figure.

larly proposed as the vanishing of long-time relaxation dynamics above "absolute zero temperature" in the volume fraction space – the latter being where all dynamics vanish, including short-time self diffusion (the point at which all dynamics vanish in colloids is not well established or agreed; some infer it occurs with crystallization[71] while others argue it occurs at random-close packing[77,147]). Nonetheless, the existence of an ideal glass transition has not been verified, and using it as an assumption is problematic. Instead, one should quench to as high volume fraction as possible and directly observe the dynamical behavior in the intransient state. If the relaxation time deviates from a divergent fit, one can conclude that there is no smooth transition to divergence.

Next, we plot the relaxation time in the intransient state as a function of volume fraction. **Figure 9** shows the relaxation time computed in our simulations — both from the MSD (green filled circles) and from the SISF (red filled circles). Alongside our data we show data reported elsewhere in the literature[2,98,148,149]. Our results agree well with the literature data. Testing for divergence requires a closer look at the region $0.50 \leq \phi \leq 0.60$, which is plotted in the inset. The relaxation timescales measured by both MSD and SISF show the same behavior for $\phi < 0.56$, which supports our claim that the MSD and the SISF are equivalent in this regime. At $\phi \geq 0.56$, we expect the two measures to differ because the cage size (probed by the MSD) is no longer equivalent to a particle

size (probed by the SISF at $qa = 3.25$), and we indeed observe the separation of two relaxation times in the inset. Strikingly, the relaxation time extracted from the SISF starts to deviate from the VFT scaling at $\phi \geq 0.58$ — growth slows — and the softening growth of relaxation time measured by MSD is even more pronounced. That is, dynamics are faster than predicted by VFT scaling. The apparent turnover of the curves occurs at the volume fraction where we predict the emergence of dense diffusion, at $\phi \rightarrow 0.59$, and indicates that relaxation time remains finite.

Polydispersity is well-known to shift to higher volume fractions the onset of glassy behavior. In the present study, we selected a polydispersity of 7% that, according to theoretical estimates, should lead to vanishing dynamics before $\phi = 0.585$[67]. Clearly this arrest is absent. Thus, even taking into account the effects of polydispersity, we find that dynamics re-emerge well beyond $\phi_{g,MCT}$, and that the relaxation time remains finite well into the putative glass.

Finally, to fully connect this finite relaxation to self-motion, we plot the inverse of an estimated long-time self-diffusion coefficient in the inset of **Figure 9**. It follows a similar concentration dependence as does the MSD and the SISF, consistent with a marked deviation from the VFT function, which indicates finite relaxation via single-particle dynamics.

Thus far we have confined our discussion to $\phi \leq 0.595$, where it is not too difficult to reach an intransient state; in all cases, diffusive dynamics re-emerge in well-defined terminal state, permitting direct measurement of the relaxation time. Relaxation remains finite for all $\phi \leq 0.595$, casting out the notion of a point at which long-time dynamics vanish. More fundamentally, our results indicate that the shift in dynamics is not an "ideal" glass transition, up to at least $\phi = 0.595$. In fact, there is only a smooth, gradual transition in dynamics: the key features (intransient terminal regime, emergence of long-time self-diffusin, finite relaxation time) are similar throughout the range $0.51 \leq \phi \leq 0.595$ (**cf Figure 3**). The smooth, gradual transition from liquid-like dynamics to aging dynamics to strongly glassy dynamics suggests that even at higher volume fractions, $\phi > 0.595$, dynamics persist. In addition, it would be surprising if the turnover of the relaxation time in the inset of **Figure 9** were to reverse at higher volume fractions prior to maximum packing.

We now examine quenches beyond the previously identified glass transition point, by conducting deeper quenches into the glass. We present particle dynamics as they evolve over time after quenches from $\phi = 0.50$ to final volume fractions $0.56 \leq \phi \leq 0.63$ in **Figure 10**. Panels (a) and (b) are simulation data starting at age $6,000 a^2/D$ after the quench. The long-time dynamics clearly emerge following the glassy plateau, for all volume fractions, even at $\phi = 0.63$. The trend of the curves suggests that at longer times (older ages), the curves could become fully linear. If an intransient state exists, we thus expect that the long-time dynamics are diffusive in what is perhaps a metastable state, similar to what was shown above in **Figure 4**. However, since simulations were not run long enough for $\phi \geq 0.60$, we do not demonstrate that an intransient state exists beyond $\phi = 0.60$, a perennial challenge very deep into the glass where the system is out of equilibrium. Nonetheless, the linear growth of MSD indicates continued
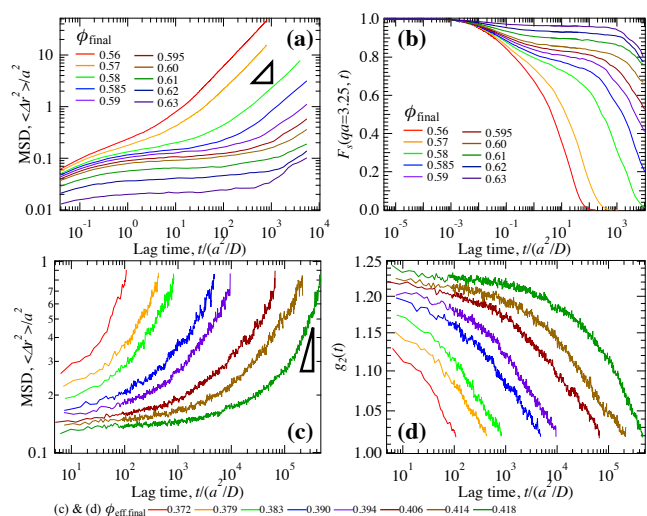
Fig. 10 (a) Mean-square displacement as a function of lag time at the wait time isochrone of 6,000 a^2/D for volume fraction jumps from $\phi_{initial} = 0.50$ to different final volume fractions within the range of 0.56-0.63. The results are averaged over five independent realizations for each jump. (b) Self-intermediate scattering function as a function of lag time at the same wait time isochrone for volume fraction jumps from $\phi_{initial} = 0.50$ to different final volume fractions within the range of 0.56-0.595. (c) "Equilibrium" mean-square displacement from PS-PNIPAM particles experiments. "Equilibrium" here means that an intransient state which no longer depends on wait time. (d) "Equilibrium" intensity autocorrelation g_2 from PS-PNIPAM particles experiments.

emergence of decorrelated particle motion above $\phi = 0.60$, and its emergence from a small cage size supports the model put forth here that "dense diffusion" within a small but configurationally dense region relaxes the glass, arguably toward an intransient state. Fluctuations in the long-time data become noticeable beyond $\phi = 0.60$, which we believe reflects the physics of strongly hindered relaxation: in our model of short-range, long-time diffusion, the statistical sampling of the dense configuration space has slowed down due to strongly restricted particle mobility. More realizations of the simulation (or, equivalently, larger system size) should reduce this noise. Overall these results for relaxation at very high volume fractions confirm that individual particle dynamics continue to relax the structure well into the glass, that dynamics do not vanish up to $\phi = 0.63$, and that the model put forth here of a dense diffusion regime explains the short-distance, long-time dynamics that produce this relaxation.

Panels (c) and (d) of **Figure 10** are experimental data from the present study; the MSDs are shown in Panel (c), and the intensity autocorrelation functions g_2 are shown in Panel (d). In our PS-PNIPAM experiments, each volume fraction can reach a stationary "equilibrium" state, yet the long-time dynamics are not completely suppressed either; in fact the long-time dynamics remain quite diffusive for all volume fractions explored, possibly due to softness of the particles that allows additional relaxation modes via deformation [150]. The intensity autocorrelation function measured in experiments agrees qualitatively with the SISF measured in the simulations, in terms of the emergence of a plateau, where an upward shift of both sets of curves with increasing vol-

ume fraction corresponds to the downward shift of the MSD, and the lengthening of the plateau corresponding to tighter cages. These results provide further supporting evidence that there is still small-scale particle rearrangement in these 'glassy' systems, and it drives ongoing system relaxation.

In summary, deep into the glassy regime, long-time self-diffusion still emerges, in the form of a "dense diffusion" regime, in contrast to the long-range motion in the liquid regime. The relaxation dynamics slow down with volume fraction, but also occur over a shorter length scale, that is a "cage" size much smaller than the particle size, thus the relaxation time does not diverge before random close packing. While particles can move infinitely far away from their initial position to sample configurations in a mobile suspension, in glassy systems particles are restricted in a small volume; instead, they cascade configurations to their neighbors, essentially allowing the tracer far away to sample the entire configurational space. This process eventually ceases when the slowing down of dynamics outweighs the increase of density of configurations, corresponding to a full dynamical arrest at random close packing.

4 Discussion and Conclusions

We have conducted a detailed computational study of the colloidal glass transition in a model colloidal glass, accompanied by experiments. Despite decades of study, the location and mechanistic process of colloidal vitrification has remained murky. While Mode Coupling Theory demonstrated the qualitative result of divergent growth of relaxation time observed in experiments, MCT substantially under-predicted the volume fraction of divergence, $\phi_{g,MCT} = 0.525$. Although *ad hoc* modification of MCT to account for size polydispersity, particle roughness, and hydrodynamic effects revised the value to $\phi_{g,MCT} \approx 0.581$, more or less to match experimental observations, experimentally-obtained values for the glass transition point are the product of extrapolation using a fitting function that *prescribes* divergence of the relaxation time; different functional forms of divergence trivially change the glass transition point. Meanwhile, a separate avenue of inquiry aimed to correct MCT's under-prediction by incorporating an activated relaxation process that permits relaxation for $\phi > 0.525$ but slows divergently with increasing volume fraction. RFOT and ABHT each hypothesize cooperative motion over a distinct length scale, and a mechanistic model for how motion over this length scale grows more difficult with increasing volume fraction. For RFOT applied to colloids, the barrier to relaxation is proportional to the size of a growing particle cluster that grows to infinite size at maximum packing. However, the theory relies on the existence of an ideal glass transition that again prescribes rather than predicts divergence. ABHT's elastic cage model predicts no divergence to occur where, again, cooperative motion permits ongoing relaxation. In both cases however, the lack of evidence of cooperative dynamics leaves the mechanistic model of glassy relaxation unclear.

From this rich scientific history we identified four primary unresolved issues: (1) whether cooperative motion drives colloidal glassy relaxation processes; (2) whether relaxation time formally diverges and, if so, at what volume fraction; (3) what process

enables dynamics to decorrelate within the putative glass region; (4) what is the driving force for such dynamical process? These remain unresolved because divergence is prescribed and the co-operative motion claimed to be the mechanism of relaxation requires large-scale structure or dynamics not observed. Both errors emerge from the difficulty of quenching deep into the glass and of making detailed observations of individual particle motion. In the present study we leveraged the power of dynamic simulations to overcome these barriers, and constructed a novel size-jump algorithm and to quench deep into the glass, while monitoring the displacements of 55,000 hard-sphere colloids during and following the quench.

We first examined the consensus [28,35,36,38,71,76] that collective motion within dynamically heterogeneous regions of several particle sizes drives glassy relaxation in colloids – an assertion not supported with measurements. To interrogate this idea, we measured and compared the self- and coherent-intermediate scattering function over length scales larger than one particle size. Prior studies focus on the wave number corresponding to motion over a single particle size, but we recognized that motion over that length scale is at best an ambiguous indication of cooperative motion. We measured the CISF and SISF over a range of wave numbers, finding that the magnitude of the CISF is very small compared to the SISF, from which we conclude that there are no appreciable collective dynamics for structures larger than a particle size, and surmised that long-time relaxation occurs via long-time self-diffusion.

Having eliminated large-scale collective motion as the primary relaxation mechanism, we shifted our focus to how single-particle dynamics evolve in the glass. While most experiments search for divergent relaxation time by examining the SISF at a single wave number corresponding to motion of a particle size, we recognized that relaxation occurs over many length scales in a concentrated dispersion. We thus measured the mean-square displacement, which automatically probes many length scales, and comparison of SISF to MSD at various quench depths and at long wait times (ages) uncovered four important results: first, we demonstrated that colloidal self-diffusion drives relaxation to the intransient state; second, such diffusion persists deep into the glass even up to $\phi = 0.63$; third, the range of diffusive motion corresponds to a cage size that is only a fraction of a particle size, and shrinks with quench depth; and fourth, there is a breakdown in the equivalence between cage size and particle size.

The plateau height in the MSD reveals the physical cage size; it is much smaller than a particle size and shrinks with quench depth — but not with age — explaining the decoupling of the SISF and the MSD. But even though particle dynamics slow dramatically as colloidal volume fraction increases, we show that the length scale over which decorrelation occurs also shrinks, permitting long-time diffusive relaxation well above $\phi_{g,MCT}$. From these results we showed that colloidal glassy relaxation occurs via a two-step process comprising correlated self-motion that melts the glassy plateau, followed by short-range, long-time self-diffusion that relaxes the glass to the intransient state.

We thus propose that the colloidal glass transition is a shift from long-ranged, long-time self-diffusion to *short-ranged*, long-time self-diffusion, where a particle need travel smaller and smaller distances to explore many configurations and decorrelate its motion. As particle volume fraction increases, the densely packed structure does indeed reduce particle mobility, but also densifies the local configurational space. Thus, long-time self-diffusion still emerges as particles sample different configurations, but requires them to explore only a very small volume. All particles in the glass execute similar local exploration, cascading many configurations from the far field toward a test particle, allowing the tracer to sample the entire suspension without wandering far from its starting point. We refer to this short-range, long-time exploration of dense configuration space as dense diffusion.

Our finding that the increasing density of configuration space underlies the persistence of relaxation deep into the glass suggests an entropic driving force — possibly related to a continued search for crystalline structure. The fact that colloidal glassy relaxation dynamics do not occur with diverging length or time scales, but rather emerge at shorter and shorter length scales, casts out the idea that the glass transition is a thermodynamic transition. An examination of osmotic pressure and coordination number may be more revealing of this driving force.

In terms of outlook, the natural next step is to explore the role played by hydrodynamic interactions, particle softness, or particle roughness, the latter being straightforward to model via a WCA/harmonic/Hertzian soft potential. This would potentially improve direct comparison to experimental systems. Future study should also explore the role of polydispersity in the dynamic "changeover" regime, whether hard particles in experiments can more closely match simulation results, and the role of hydrodynamic interactions on the transition itself.

Conflicts of interest

There are no conflicts to declare.

Acknowledgements

Notes and references

1 M. Aegerter and M. Mennig, *Sol-Gel Technologies for Glass Producers and Users*, 2004.

2 G. L. Hunter and E. R. Weeks, *Rep. Prog. Phys.*, 2012, **75**, 066501.

3 P. J. Lu and D. A. Weitz, *Annu. Rev. Condens. Matter Phys.*, 2013, **4**, 217–233.

4 B. R. Parry, I. V. Surovtsev, M. T. Cabeen, C. S. OâĂŹHern,

E. R. Dufresne and C. Jacobs-Wagner, *Cell*, 2014, **156**, 183 – 194.

5   L. Slade, H. Levine, J. Ievolella and M. Wang, *Journal of the Science of Food and Agriculture*, 1993, **63**, 133–176.

6   Y. H. Roos, *Annual Review of Food Science and Technology*, 2010, **1**, 469–496.

7   E. Zaccarelli, *J. Phys.: Condens. Matter*, 2007, **19**, 323101.

8   W. Vogel, in *Glass Chemistry*, ed. W. Vogel, Springer Berlin Heidelberg, Berlin, Heidelberg, 1994, pp. 280–362.

9   R. N. Zia, B. J. Landrum and W. B. Russel, *J. Rheol.*, 2014, **58**, 1121–1157.

10 B. J. Landrum, W. B. Russel and R. N. Zia, *J. Rheol.*, 2016, **60**, 783–807.

11 P. Padmanabhan and R. Zia, *Soft Matter*, 2018, **14**, 3265–3287.

12 R. Kohlrausch, *Annalen der Physik*, 1854, **167**, 56–82.

13 H. L. La Chatellier, *Comptes rendus*, 1884, **99**, 786âĂŞ789.

14 A. Q. Tool and C. G. Eichlin., *J. Opt. Soc. Am.*, 1920, **4**, 340–363.

15 H. Vogel, *Z. Phys.*, 1921, **22**, 645–6.

16 G. S. Fulcher, *J. Am. Ceram. Soc.*, 1925, **8**, 339–355.

17 G. Tammann and W. Hesse, *Zeitschrift fÃijr anorganische und allgemeine Chemie*, 1926, **156**, 245–257.

18 F. Simon, in *Schriftleitung der âĂđNaturwissenschaftenâĂİ (eds) Ergebnisse der Exakten Naturwissenschaften*, Springer, Berlin Heidelberg, 1930.

19 F. Simon, *Zeitschrift fÃijr anorganische und allgemeine Chemie*, 1931, **203**, 219–227.

20 W. Kauzmann, *Chemical Reviews*, 1948, **43**, 219–256.

21 I. M. Krieger and T. J. Dougherty, *Transactions of the Society of Rheology*, 1959, **3**, 137–152.

22 A. J. Kovacs, in *Fortschritte Der Hochpolymeren-Forschung*, Springer, Berlin Heidelberg, 1964, ch. 3.

23 G. Adam and J. H. Gibbs, *J. Chem. Phys.*, 1965, **43**, 139–146.

24 J. H. Gibbs and E. A. DiMarzio, *J. Chem. Phys.*, 1958, **28**, 373–383.

25 M. Goldstein, *The Journal of Chemical Physics*, 1969, **51**, 3728–3739.

26 G. Williams and D. C. Watts, *Trans. Faraday Soc.*, 1970, **66**, 80–85.

27 U. Bengtzelius, W. Götze and A. Sjölander, *Journal of Physics C: Solid State Physics*, 1984, **17**, 5915–5934.

28 W. Götze and L. Sjögren, *Rep. Prog. Phys*, 1992, **55**, 241.

29 P. N. Pusey and W. van Megen, *Nature*, 1986, **320**, 340–342.

30 P. N. Pusey and W. van Megen, *Phys. Rev. Lett.*, 1987, **59**, 2083–2086.

31 T. R. Kirkpatrick and P. G. Wolynes, *Phys. Rev. A*, 1987, **35**, 3072–3080.

32 T. R. Kirkpatrick and P. G. Wolynes, *Phys. Rev. B*, 1987, **36**, 8552–8564.

33 T. R. Kirkpatrick and D. Thirumalai, *Phys. Rev. B*, 1988, **37**, 5342–5350.

34 T. R. Kirkpatrick and D. Thirumalai, *Phys. Rev. A*, 1988, **37**, 4439–4448.

35 T. R. Kirkpatrick, D. Thirumalai and P. G. Wolynes, *Phys. Rev. A*, 1989, **40**, 1045–1054.

36 K. S. Schweizer and E. J. Saltzman, *The Journal of Chemical Physics*, 2003, **119**, 1181–1196.

37 K. S. Schweizer, *The Journal of Chemical Physics*, 2005, **123**, 244501.

38 S. Mirigian and K. S. Schweizer, *The Journal of Chemical Physics*, 2014, **140**, 194506.

39 S. Mirigian and K. S. Schweizer, *The Journal of Chemical Physics*, 2014, **140**, 194507.

40 P. Ramírez-González and M. Medina-Noyola, *Phys. Rev. E*, 2010, **82**, 061503.

41 P. Pusey, W. V. Megen, S. Underwood, P. Bartlett and R. Ottewill, *Physica A*, 1991, **176**, 16 – 27.

42 W. Härtl, *Curr. Opin. Colloid Interface Sci.*, 2001, **6**, 479 – 483.

43 W. C. Poon, *MRS Bulletin*, 2004, **29**, 96âĂŞ99.

44 F. Sciortino and P. Tartaglia, *Adv. Phys.*, 2005, **54**, 471–524.

45 P. N. Pusey, *J. Phys.: Condens. Matter*, 2008, **20**, 494202.

46 E. Zaccarelli and W. C. K. Poon, *Proc. Natl. Acad. Sci.*, 2009, **106**, 15203–15208.

47 D. A. Weitz, in *Glasses and Grains: Poincaré Seminar 2009*, ed. B. Duplantier, T. C. Halsey and V. Rivasseau, Springer Basel, Basel, 2011, pp. 25–39.

48 L. Berthier and G. Biroli, *Rev. Mod. Phys.*, 2011, **83**, 587–645.

49 Y. M. Joshi, *Annu. Rev. Chem. Biomol. Eng.*, 2014, **5**, 181–202.

50 E. R. Weeks, *ACS Macro Lett.*, 2017, **6**, 27–34.

51 W. van Megen and S. M. Underwood, *Phys. Rev. E*, 1994, **49**, 4206–4220.

52 W. van Megen, T. C. Mortensen, S. R. Williams and J. Müller, *Phys. Rev. E*, 1998, **58**, 6073–6085.

53 G. Brambilla, D. El Masri, M. Pierno, L. Berthier, L. Cipelletti, G. Petekidis and A. B. Schofield, *Phys. Rev. Lett.*, 2009, **102**, 085703.

54 I. M. Krieger, *Advances in Colloid and Interface Science*, 1972, **3**, 111 – 136.

55 C. G. de Kruif, E. M. F. van Iersel, A. Vrij and W. B. Russel, *The Journal of Chemical Physics*, 1985, **83**, 4717–4725.

56 J. Mewis, W. J. Frith, T. A. Strivens and W. B. Russel, *AIChE Journal*, 1989, **35**, 415–422.

57 T. Shikata and D. S. Pearson, *J. Rheol.*, 1994, **38**, 601–616.

58 P. N. Segrè, S. P. Meeker, P. N. Pusey and W. C. K. Poon, *Phys. Rev. Lett.*, 1995, **75**, 958–961.

59 S.-E. Phan, W. Russel, Z. Cheng, J. Zhu, P. Chaikin, J. Dunsmuir and R. Ottewill, *Physical Review E*, 1996, **54**, 6633–6645.

60 S. P. Meeker, W. C. K. Poon and P. N. Pusey, *Phys. Rev. E*, 1997, **55**, 5718–5722.

61 B. J. Maranzano and N. J. Wagner, *J. Rheol.*, 2001, **45**, 1205–1222.

62 Z. Cheng, J. Zhu, P. M. Chaikin, S.-E. Phan and W. B. Russel, *Phys. Rev. E*, 2002, **65**, 041405.

63 S. Henderson, T. Mortensen, S. Underwood and W. van Megen, *Physica A: Statistical Mechanics and its Applications*, 1996, **233**, 102 – 116.

64 S. R. Williams and W. van Megen, *Phys. Rev. E*, 2001, **64**, 041502.

65 H. J. Schŭpe, G. Bryant and W. van Megen, *The Journal of Chemical Physics*, 2007, **127**, 084505.

66 P. N. Pusey, E. Zaccarelli, C. Valeriani, E. Sanz, W. C. K. Poon and M. E. Cates, *Philosophical Transactions of the Royal Society A: Mathematical, Physical and Engineering Sciences*, 2009, **367**, 4993–5011.

67 W. van Megen and S. R. Williams, *Phys. Rev. Lett.*, 2010, **104**, 169601.

68 E. Zaccarelli, S. M. Liddle and W. C. K. Poon, *Soft Matter*, 2015, **11**, 324–330.

69 J. Yang and K. S. Schweizer, *J. Chem. Phys.*, 2011, **134**, 204908.

70 A.-M. Philippe, D. Truzzolillo, J. Galvan-Myoshi, P. Dieudonné-George, V. Trappe, L. Berthier and L. Cipelletti, *Phys. Rev. E*, 2018, **97**, 040601.

71 T. R. Kirkpatrick and D. Thirumalai, *Rev. Mod. Phys.*, 2015, **87**, 183–209.

72 C. Donati, J. F. Douglas, W. Kob, S. J. Plimpton, P. H. Poole and S. C. Glotzer, *Phys. Rev. Lett.*, 1998, **80**, 2338–2341.

73 E. R. Weeks, J. C. Crocker, A. C. Levitt, A. Schofield and D. A. Weitz, *Science*, 2000, **287**, 627–631.

74 A. D. S. Parmar, S. Sengupta and S. Sastry, *Phys. Rev. Lett.*, 2017, **119**, 056001.

75 A. J. Banchio, G. Nägele and J. Bergenholtz, *J. Chem. Phys.*, 1999, **111**, 8721–8740.

76 V. Lubchenko and P. G. Wolynes, *Annu. Rev. Phys. Chem.*, 2007, **58**, 235–266.

77 W. B. Russel, N. J. Wagner and J. Mewis, *J. Rheol.*, 2013, **57**, 1555–1567.

78 P. Mendoza-Méndez, E. Lázaro-Lázaro, L. E. Sánchez-Díaz, P. E. Ramírez-González, G. Pérez-Ángel and M. Medina-Noyola, *Phys. Rev. E*, 2017, **96**, 022608.

79 A. K. Doolittle, *Journal of Applied Physics*, 1951, **22**, 1471–1475.

80 A. Cavagna, *Physics Reports*, 2009, **476**, 51 – 124.

81 G. K. Batchelor, *Journal of Fluid Mechanics*, 1976, **74**, 1–29.

82 G. K. Batchelor, *Journal of Fluid Mechanics*, 1983, **131**, 155–175.

83 L. V. Woodcock, *Annals of the New York Academy of Sciences*, 1981, **371**, 274–298.

84 J. M. Rallison, *Journal of Fluid Mechanics*, 1988, **186**, 471–500.

85 M. Medina-Noyola, *Phys. Rev. Lett.*, 1988, **60**, 2705–2708.

86 J. A. Leegwater and G. Szamel, *Phys. Rev. A*, 1992, **46**, 4999–5011.

87 J. F. Brady, *Journal of Fluid Mechanics*, 1994, **272**, 109–134.

88 J. M. Rallison and E. J. Hinch, *J. Fluid Mech.*, 1986, **167**, 131–168.

89 L. Yeomans-Reyna and M. Medina-Noyola, *Phys. Rev. E*, 2001, **64**, 066114.

90 J. Zhao, S. L. Simon and G. B. McKenna, *Nat. Commun.*, 2013, **4**, 1783.

91 H. Yoon and G. B. McKenna, *Sci. Adv.*, 2018, **4**, 12.

92 L. C. E. Struik, *Physical aging in amorphous polymers and other materials*, Elsevier Scientific Pub. Co. ; distributors for the U.S. and Canada, Elsevier North-Holland Amsterdam ; New York : New York, 1978, pp. xiv, 229 p. :.

93 G. B. McKenna, *J. Phys.: Condens. Matter*, 2003, **15**, S737–S763.

94 D. J. Lacks and M. J. Osborne, *Phys. Rev. Lett.*, 2004, **93**, 255501.

95 W. van Megen and S. M. Underwood, *Nature*, 1993, **362**, 616–618.

96 X. Peng and G. B. McKenna, *Phys. Rev. E*, 2014, **90**, 050301.

97 R. E. Courtland and E. R. Weeks, *J. Phys.: Condens. Matter*, 2003, **15**, S359.

98 D. El Masri, G. Brambilla, M. Pierno, G. Petekidis, A. B. Schofield, L. Berthier and L. Cipelletti, *J. Stat. Mech. Theory Exp.*, 2009, **2009**, P07015.

99 A. Q. Tool, *J. Res. Nat. Bureau Stds*, 1945, **34**, 199–211.

100 O. S. Narayanaswamy, *J. Am. Ceram. Soc.*, 1971, **54**, 491–498.

101 C. T. Moynihan, P. B. Macedo, C. J. Montrose, C. J. Montrose, P. K. Gupta, M. A. DeBolt, J. F. Dill, B. E. Dom, P. W. Drake, A. J. Easteal, P. B. Elterman, R. P. Moeller, H. Sasabe and J. A. Wilder, *Ann. New York Acad. Sci.*, 1976, **279**, 15–35.

102 A. J. Kovacs, J. J. Aklonis, J. M. Hutchinson and A. R. Ramos, *J. Polym. Sci. B: Polym. Phys.*, 1979, **17**, 1097–1162.

103 X. Di, K. Z. Win, G. B. McKenna, T. Narita, F. Lequeux, S. R. Pullela and Z. Cheng, *Phys. Rev. Lett.*, 2011, **106**, 095701.

104 X. Di, X. Peng and G. B. McKenna, *J. Chem. Phys.*, 2014, **140**, 054903.

105 X. Peng and G. B. McKenna, *Phys. Rev. E*, 2016, **93**, 042603.

106 Q. Li, X. Peng and G. B. McKenna, *Soft Matter*, 2017, **13**, 1396–1404.

107 Q. Li, X. Peng and G. B. McKenna, *Soft Matter*, 2019, **15**, 2336–2347.

108 X. Peng, J. G. Wang, Q. Li, D. Chen, R. N. Zia and G. B. McKenna, *Phys. Rev. E*, 2018, **98**, 062602.

109 S. Plimpton, *J. Comput. Phys.*, 1995, **117**, 1 – 19.

110 R. N. Zia, J. W. Swan and Y. Su, *J. Chem. Phys.*, 2015, **143**, 224901.

111 J. BERGENHOLTZ, J. F. BRADY and M. VICIC, *J. Fluid Mech.*, 2002, **456**, 239–275.

112 A. S. KHAIR and J. F. BRADY, *J. Fluid Mech.*, 2006, **557**, 73–117.

113 A. S. Khair, M. Swaroop and J. F. Brady, *Phys. Fluids*, 2006, **18**, 043102.

114 M. Swaroop and J. F. Brady, *J. Rheol.*, 2007, **51**, 409–428.

115 A. Brünger, C. L. Brooks and M. Karplus, *Chem. Phys. Lett.*,

Soft Matter Accepted Manuscript

1984, **105**, 495 – 500.

116 M. Cloitre, R. Borrega and L. Leibler, *Phys. Rev. Lett.*, 2000, **85**, 4819–4822.

117 L. Cipelletti and L. Ramos, *Journal of Physics: Condensed Matter*, 2005, **17**, R253–R285.

118 E. H. Purnomo, D. van den Ende, S. A. Vanapalli and F. Mugele, *Phys. Rev. Lett.*, 2008, **101**, 238301.

119 J. Mattsson, H. M. Wyss, A. Fernandez-Nieves, K. Miyazaki, Z. Hu, D. R. Reichman and D. A. Weitz, *Nature*, 2009, **462**, 83–86.

120 S. A. Rogers, P. T. Callaghan, G. Petekidis and D. Vlassopoulos, *Journal of Rheology*, 2010, **54**, 133–158.

121 J. R. Seth, L. Mohan, C. Locatelli-Champagne, M. Cloitre and R. T. Bonnecaze, *Nat. Mater.*, 2011, **10**, 838–843.

122 B. M. Erwin, D. Vlassopoulos, M. Gauthier and M. Cloitre, *Phys. Rev. E*, 2011, **83**, 061402.

123 L. Mohan, R. T. Bonnecaze and M. Cloitre, *Phys. Rev. Lett.*, 2013, **111**, 268301.

124 D. Vlassopoulos and M. Cloitre, *Curr. Opin. Colloid Interface Sci.*, 2014, **19**, 561 – 574.

125 L. Mohan, M. Cloitre and R. T. Bonnecaze, *Journal of Rheology*, 2015, **59**, 63–84.

126 M. E. A. Zakhari, P. D. Anderson and M. Hütter, *Phys. Rev. E*, 2017, **96**, 012604.

127 M. E. A. Zakhari, M. HÃijtter and P. D. Anderson, *J. Rheol.*, 2018, **62**, 831–843.

128 N. F. Carnahan and K. E. Starling, *J. Chem. Phys.*, 1969, **51**, 635–636.

129 R. J. Speedy, *J. Chem. Phys.*, 1994, **100**, 6684–6691.

130 M. D. Rintoul and S. Torquato, *J. Chem. Phys.*, 1996, **105**, 9258–9265.

131 D. R. Foss and J. F. Brady, *J. Rheol.*, 2000, **44**, 629–651.

132 M. Swaroop, *Ph.D. thesis*, California Institute of Technology, 2010.

133 M. P. Allen and D. J. Tildesley, *Computer Simulation of Liquids*, Oxford: Clarendon Press, 1987.

134 D. M. Heyes and J. R. Melrose, *J. Non-Newtonian Fluid Mech.*, 1993, **46**, 1–28.

135 T. Eckert and W. Richtering, *J. Chem. Phys.*, 2008, **129**, 124902.

136 J. J. Crassous, M. Ballauff, M. Drechsler, J. Schmidt and Y. Talmon, *Langmuir*, 2006, **22**, 2403–2406.

137 G. Romeo, A. Fernandez-Nieves, H. M. Wyss, D. Acierno and D. A. Weitz, *Adv. Mater.*, 2010, **22**, 3441–3445.

138 V. Viasnoff, F. Lequeux and D. J. Pine, *Rev. Sci. Instrum.*, 2002, **73**, 2336–2344.

139 D. A. Weitz and D. J. Pine, in *Dynamic Light Scattering*, ed. W. Brown, Oxford University Press, New York, 1993, ch. 16, pp. 652–720.

140 F. Cardinaux, L. Cipelletti, F. Scheffold and P. Schurtenberger, *Europhys. Lett.*, 2002, **57**, 738.

141 M. Wang and J. F. Brady, *Phys. Rev. Lett.*, 2015, **115**, 158301.

142 S. Banik and G. B. McKenna, *Phys. Rev. E*, 2018, **97**, 062601.

143 K. S. Schweizer and E. J. Saltzman, *J. Phys. Chem. B*, 2004, **108**, 19729–19741.

144 S. K. Kumar, G. Szamel and J. F. Douglas, *J. Chem. Phys.*, 2006, **124**, 214501.

145 S.-H. Chong and W. Kob, *Phys. Rev. Lett.*, 2009, **102**, 025702.

146 L. Berthier, D. Chandler and J. P. Garrahan, *Europhys. Lett. (EPL)*, 2005, **69**, 320–326.

147 G. Parisi and F. Zamponi, *J. Chem. Phys.*, 2005, **123**, 144501.

148 J. J. Crassous, L. Casal-Dujat, M. Medebach, M. Obiols-Rabasa, R. Vincent, F. Reinhold, V. Boyko, I. Willerich, A. Menzel, C. Moitzi, B. Reck and P. Schurtenberger, *Langmuir*, 2013, **29**, 10346–10359.

149 G. Pérez-Angel, L. E. Sánchez-Díaz, P. E. Ramírez-González, R. Juárez-Maldonado, A. Vizcarra-Rendón and M. Medina-Noyola, *Phys. Rev. E*, 2011, **83**, 1–4.

150 B. M. Erwin, M. Cloitre, M. Gauthier and D. Vlassopoulos, *Soft Matter*, 2010, **6**, 2825–2833.